

Kinetic freeze-out properties in relativistic heavy ion collisions from RHIC Beam Energy Scan to LHC

Jia Chen,^{1,2} Jian Deng,^{1,2} Zebo Tang,³ Zhangbu Xu,⁴ and Li Yi^{1,2,*}

¹*Institute of Frontier and Interdisciplinary Science,*

Shandong University, Qingdao, Shandong, 266237, China

²*Key Laboratory of Particle Physics and Particle Irradiation,
Ministry of Education, Shandong University, Qingdao, Shandong, 266237, China*

³*State Key Laboratory of Particle Detection and Electronics,*

University of Science and Technology of China, Hefei, Anhui, 230026, China

⁴*Brookhaven National Laboratory, Upton, New York, 11973, USA*

(Dated: December 22, 2024)

In this paper, we investigate the kinetic freeze-out properties in relativistic heavy ion collisions at different collision energies. We present a study of standard Boltzmann-Gibbs Blast-Wave (BGBW) fits and Tsallis Blast-Wave (TBW) fits performed on the transverse momentum spectra of identified hadrons produced in Au + Au collisions at collision energies of $\sqrt{s_{NN}} = 7.7 - 200$ GeV at Relativistic Heavy Ion Collider (RHIC), and in Pb + Pb collisions at collision energies of $\sqrt{s_{NN}} = 2.76$ and 5.02 TeV at the Large Hadron Collider (LHC). The behavior of strange and multi-strange particles is also investigated. We found that the TBW model describes data better than the BGBW one overall, and the contrast is more prominent as the collision energy increases as the degree of non-equilibrium of the produced system is found to increase. From TBW fits, the kinetic freeze-out temperature at the same centrality shows a weak dependence of collision energy between 7.7 and 39 GeV, while it decreases as collision energy continues to increase up to 5.02 TeV. The radial flow is found to be consistent with zero in peripheral collisions at RHIC energies but sizable at LHC energies and central collisions at all RHIC energies. We also observed that the strange hadrons, with higher temperature and similar radial flow, approach equilibrium more quickly from peripheral to central collisions than light hadrons. The dependence of temperature and flow velocity on non-equilibrium parameter ($q - 1$) is characterized by two second-order polynomials. Both a and $d\xi$ from the polynomials fit, related to the influence of the system bulk viscosity, increases toward lower RHIC energies.

I. INTRODUCTION

Relativistic heavy ion collisions can create extreme hot and dense matter and reach a phase transition to Quark-Gluon Plasma (QGP). As QGP expands rapidly, its temperature drops and the system starts to enter hadronic phase. Eventually the system reaches kinetic freeze-out when all particle interactions cease. The particle spectra are thus frozen, which carry information about system dynamics at that freeze-out and even earlier. Therefore, the study of differential transverse momentum (p_T) distributions of hadron particles is an useful tool to look into the evolution of the system, especially to extract system properties at its freeze-out phase space. Boltzmann-Gibbs Blast-Wave (BGBW) model [1, 2] has been widely used to describe the produced system at kinetic freeze-out with its system-wise parameters characterizing the system radial flow velocity and temperature.

The BGBW model assumes that the produced system has reached local thermal equilibrium so that a Boltzmann distribution with a radial flow profile can be used to describe the particle spectra [1]. However, the equilibrium distribution can only describes the very limited

low p_T spectra and is sensitive to the choice of a specific p_T range. Tsallis statistics was introduced later in the literature to describe the particle production for an extended p_T range in high energy collisions [3–8]. One advantage of those Tsallis statistical analyses compared to Boltzmann-Gibbs statistical one is that a new parameter is introduced in the model to describe the degree of non-equilibrium in the system, which is especially helpful for $p + p$ collisions [9] and peripheral A+A collisions. Some papers [10] proposed a possible microcanonical generalization of the Tsallis distribution which gives a good fit to data on fragmentation functions measured in e^+e^- collisions for $0.01 \leq x \leq 1$.

The energy dependence of radial flow velocity and kinetic freeze-out temperature in high energy heavy ion collisions has been an interesting subject in the community and been extensively studied for all collision energies. In the energy range of the Heavy Ion Synchrotron (SIS) to Super Proton Synchrotron (SPS), multiple studies agreed on an increasing trend for those two variables with an increase of the collision energy [11, 16, 17]. From RHIC to the LHC energy range, however, the interpretation of the experimental results are model dependent to date. For radial flow velocity, most studies found an increasing trend of flow velocity with increasing collision energy [11–17] but the quantitative value and whether

* li.yi@sdu.edu.cn

there is sizable flow in p+p and peripheral A+A collisions are model dependent. For kinetic freeze-out temperature, some studies claimed an increasing trend of kinetic freeze-out temperature with increasing collision energy [13, 14] while others stated a decreasing trend [16–20], and some concluded little dependence on collision energy [11, 12].

In this paper, to extract kinetic freeze-out temperature and radial flow velocity, we use blast-wave model with Tsallis statistics [21–23] and compare to Boltzmann-Gibbs statistics one [1, 24, 25] to simultaneously fit all the transverse momentum spectra of hadrons produced at mid-(pseudo)rapidity in $\sqrt{s_{NN}} = 7.7, 11.5, 14.5, 19.6, 27, 39, 62.4$ and 200 GeV Au + Au collisions at RHIC [17, 24, 26–29, 38–44] and in $\sqrt{s_{NN}} = 2.76$ TeV [30] and 5.02 TeV [31] Pb + Pb collisions at the LHC. Such a systematic study on collision energy and centrality dependence of radial flow velocity, kinetic freeze-out temperature and the degree of non-equilibrium from RHIC to the LHC energy range may shed light on the underlying physics in these collisions. Strange and multi-strange particles, with smaller hadronic interaction cross-sections, are believed to decouple from the system earlier than hadrons with only light valence quarks. The kinetic freeze-out behaviors of strange and multi-strange particles are therefore also investigated separately.

This paper is organized as following. In Section II, we describe the analysis method used in this work. Results and discussions are given in Section III. Conclusion is summarized in the last section.

II. ANALYSIS METHOD

A. Blast-Wave model

BGBW is a phenomenological model for hadron spectra based on flowing local thermal sources with global variables of temperature T and transverse flow profile β [1, 2]. T is the temperature of the local thermal sources which particles radiate from. While the longitudinal expansion is assumed to be boost-invariant, the transverse radial flow velocity of the thermal source is parameterized as $\beta(r) = \beta_S (\frac{r}{R})^n$ at radius $0 \leq r \leq R$ with surface velocity β_S and exponent n . The average radial flow velocity then can be written as $\langle \beta \rangle = \beta_S \cdot 2/(2+n)$ [36]. For an emitting source with Boltzmann-Gibbs distribution, the produced particle spectrum is therefore written in the form of

$$\frac{d^2 N}{2\pi p_T dp_T dy} \Big|_{y=0} = A \int_0^R r dr m_T I_0\left(\frac{p_T \sinh(\rho)}{T}\right) \cdot K_1\left(\frac{m_T \cosh(\rho)}{T}\right), \quad (1)$$

where A is a normalization factor. $m_T = \sqrt{p_T^2 + m^2}$ is the transverse mass of a particle. I_0 and K_1 are the modified Bessel functions. $\rho = \tanh^{-1} \beta$. T is the kinetic freeze-out temperature. In order to compare with TBW

results, we take $n = 1$ for BGBW model in this paper. With common freeze-out temperature T and average radial flow velocity $\langle \beta \rangle$, the shape of the spectrum for each particle species is determined by its mass in BGBW.

B. Tsallis Blast-Wave model

TBW [21–23, 36] is modified from the standard BGBW model when a Tsallis statistics replaces the conventional Boltzmann-Gibbs statistics for the particle emission distribution. The invariant differential particle yield in TBW is then written in the form of

$$\frac{d^2 N}{2\pi m_T dm_T dy} \Big|_{y=0} = A \int_{-y_b}^{+y_b} e^{\sqrt{y_b^2 - y_s^2}} m_T \cosh(y_s) dy_s \times \int_0^R r dr \int_{-\pi}^{\pi} \left[1 + \frac{q-1}{T} E_T\right]^{-1/(q-1)} d\phi, \quad (2)$$

where

$$E_T = m_T \cosh(y_s) \cosh(\rho) - p_T \sinh(\rho) \cos(\phi). \quad (3)$$

y_s is the source rapidity. y_b is the beam rapidity. ϕ is the particle emission angle in the rest frame of thermal source. q is the parameter characterizing the degree of non-equilibrium of the produced system, which is the new parameter introduced in TBW compared to BGBW model. Although the applicability of such a model to high energy nuclear collisions are still under investigation, possible physics implications are available in the literature. The initial energy density in heavy ion collision has multiple hot spots caused by Color-Glass Condensate formation in a nucleon or individual nucleon-nucleon collision. Those hot spots are dissipated into the system, producing more particles, generating collective flow and resulting in a temperature fluctuation at initial state [4, 37]. The initial state fluctuation is not guaranteed to be completely washed out by the medium, in QGP or hadron gas phases. The survived fluctuation will leave imprints in spectra at low and intermediate p_T range. Such features in spectra will lead to q value larger than 1 in TBW model [36]. When $q = 1$, Eq. (2) recovers its familiar Boltzmann-Gibbs form.

In this paper, we also use a Tsallis blast-wave model with 4 fit parameters with different q for mesons and baryons separately, referred to as TBW4. TBW4 was first proposed in reference [21] for a better description of meson and baryon spectra at $p+p$ collisions while the TBW fits with one single q for all particles gave a very poor $\chi^2/nDoF$. TBW without further description in this paper refers to the default one with 3 fit parameters that is the one using the same q for both mesons and baryons.

III. RESULTS AND DISCUSSION

A. Transverse momentum spectra

This section compares three blast-wave model fits of the transverse momentum spectra. Table I lists the particle spectra data used in this paper. Those particle spectra form two species groups for the fit procedure: one with all available hadrons, another with charged pion, kaon, proton and anti-proton only. The first group is aimed to identify the common freeze-out properties for all particles. The latter is chosen to be consistent with previous publications [17] for an apple-to-apple comparison. The reported experimental systematic and statistical uncertainties are combined as quadratic sum for the fitting procedures. For all fit procedures, the average flow velocity $\langle\beta\rangle$ is limited to the range of $0 \leq \langle\beta\rangle \leq 2/3$ [24] for a better convergence in fitting and to avoid nonphysical results (negative value or fast than speed of light) [21]. Furthermore, spectra fit range is limited to $p_T \leq 3 \text{ GeV}/c$ in order to have comparable p_T range for all energies and to focus on the bulk properties. For the sake of concision, this section only shows the fits to spectra for all particles in most central and most peripheral centrality classes at four collision energies as examples in Figs. 1 to 4. Figure 1 (Figure 2) shows blast-wave fits to identified particle transverse momentum spectra in most central (most peripheral) collisions, with corresponding deviations of those fits to experimental data divided by data uncertainties shown in Fig. 3 (Fig. 4). The fit results of kinetic freeze-out parameters for both species groups at various centrality classes and collision energies are discussed in the next section. Those extracted fit parameters and $\chi^2/nDoF$ of TBW models are also summarized in Tables III to XIII.

BGBW and TBW models are compared in the left and middle panels of Figs. 1 to 4. From top to bottom panels of each figure, the spectra (Figs. 1 and 2) or difference between model and experiment data divided by the error of data (Figs. 3 and 4) in Pb + Pb or Au+Au collisions at $\sqrt{s_{NN}} = 2.76 \text{ TeV}$, 200 GeV, 62.4 GeV and 7.7 GeV are presented. At LHC and top RHIC energies, the deviation of BGBW model from experimental data is larger in peripheral than in central collisions. As beam energy decreases, the deviation of BGBW model fit from data decreases. We note that there are fewer experimental data at $p_T > 2 \text{ GeV}/c$ for energies below 39 GeV. Overall, TBW has a better fits and has smaller $\chi^2/nDoF$ than BGBW. TBW agrees with most data points within $3\text{-}\sigma$ standard deviation from experimental data. TBW yields a smaller q toward lower beam energy, which indicates that the system is closer to equilibrium state toward lower energy. For all LHC and RHIC energies, TBW fits in peripheral collisions have larger q values than those in central collisions at the same collision energy. In short, TBW model performs much better than BGBW and the non-equilibrium seems to be necessary for peripheral collisions at high energies. As BGBW model assumes ther-

mal equilibrium and TBW model uses non-equilibrium statistics, the above observations suggest that the collision system deviates more from thermal equilibrium at higher energy, especially in peripheral collisions.

The comparison of TBW (with a single q) and TBW4 (with separate q for meson and baryon) is shown in the middle and right panels of Figures 1 to 4. TBW4 has even smaller $\chi^2/nDoF$ than TBW for all LHC and RHIC energies, while the improvement is larger in peripheral than central collisions. For TBW4, the non-equilibrium parameter q of baryons is found to be smaller than that of mesons, as baryons have steeper spectra than mesons. Baryons used in the fitting include mostly strange (Λ) and multi-strange (Ξ and Ω) particle species and strangeness has smaller q value and higher freeze-out temperature. More details on different freeze-out will be discussed later in Section III B.

B. Kinetic freeze-out parameters

The extracted results for temperature T and average radial flow velocity $\langle\beta\rangle$ from BGBW, TBW and TBW4 are compared in Figs. 5 and 6. The beam energy, centrality and particle species dependences of T , $\langle\beta\rangle$, and q from TBW model are investigated in Figs. 7 and 8.

The dependence of T on $\langle\beta\rangle$ of BGBW, TBW and TBW4 are shown in Fig. 5 for charged pions, kaons and protons, and in Fig. 6 for all available hadrons including strange and multi-strange particles. Symbols with same color represent A+A collisions at same beam energy for different centrality classes. In general, fit parameters in Fig. 6 for all particles have smaller fit uncertainties than those in Fig. 5 for charged pions, kaons and protons only, as more particles are used to study their common freeze-out properties. Other than that, these two species groups give similar results for T dependence on $\langle\beta\rangle$. BGBW results shown on the left panel display an anti-correlation between T and $\langle\beta\rangle$. At the same collision energy, T decreases and $\langle\beta\rangle$ increases as system moves from peripheral to central collisions. As collision energy increases, the anti-correlation curve moves toward high $\langle\beta\rangle$. Such anti-correlation behavior was also reported in Ref. [17]. TBW results in the middle panel, however, are different from BGBW ones. T from TBW has much weaker dependence on centrality than BGBW one. For example, at the LHC energies, the increase of T from most central to most peripheral collisions is around 40% in BGBW. On the contrast, the variation of T is only about 5% in TBW. The parameter $\langle\beta\rangle$ in most central collisions from TBW is between 0.4 to 0.5 for RHIC energies and around 0.6 at the LHC, similar with those in BGBW. In peripheral collisions $\langle\beta\rangle$ is lower in TBW than that in BGBW, while it even reaches zero value for the most peripheral collisions at RHIC energies. It seems that from TBW model's viewpoint, hadron scatterings (or QGP droplets if any) are not sufficient to produce a large collective radial flow nor to maintain a thermal equilibrium in pe-

TABLE I. Spectra data references

system	$\sqrt{s_{\text{NN}}}$ (GeV)	particle	collaboration	reference
Au + Au	7.7, 11.5, 19.6, 27	$\pi^\pm, K^\pm, p, \bar{p}$	STAR	[17]
		$K_s^0, \Lambda, \bar{\Lambda}, \Xi^+, \Xi^-$	STAR	[38]
Au + Au	14.5	$\pi^\pm, K^\pm, p, \bar{p}$	STAR	[26]
Au + Au	39	$\pi^\pm, K^\pm, p, \bar{p}$	STAR	[17]
		$K_s^0, \Lambda, \bar{\Lambda}, \Xi^+, \Xi^-$	STAR	[38]
		π^0	PHENIX	[41]
Au + Au	62.4	$\pi^\pm, K^\pm, p, \bar{p}$	STAR	[24]
		π^\pm, p, \bar{p}	STAR	[27]
		$K_s^0, \Lambda, \bar{\Lambda}, \Xi^+, \Xi^-, \Omega^+, \Omega^-$	STAR	[39]
		ϕ	STAR	[40]
		π^0	PHENIX	[41]
Au + Au	200	π^\pm, p, \bar{p}	STAR	[29]
		K^\pm	STAR	[28]
		K^\pm	PHENIX	[42]
		$\Lambda, \bar{\Lambda}, \Xi^+, \Xi^-, \Omega$	STAR	[43]
Pb + Pb	2760	$\pi^\pm, K^\pm, p, \bar{p}$	STAR	[44]
		ϕ	STAR	[44]
		$\pi^\pm, K^\pm, p, \bar{p}$	ALICE	[30]
Pb + Pb	5020	K_s^0, Λ	ALICE	[45]
		$\Xi^+, \Xi^-, \Omega^+, \Omega^-$	ALICE	[46]
		$\pi^\pm, K^\pm, p, \bar{p}$	ALICE	[31]

peripheral collisions at RHIC. BGBW model, while lacking a knob for non-equilibrium degree, has to boost its radial flow parameter in a struggle to fit the high yields of the spectra at intermediate p_T in the peripheral collisions. In Figs. 5 and 6, T and $\langle\beta\rangle$ from TBW4 on the right panels are similar to those from TBW with one single q in the middle panels and different from those from BGBW on the left panels. There is a weaker centrality dependence for T and lower $\langle\beta\rangle$ values at peripheral collisions for both TBW models than BGBW. We observed that at the LHC energies, T and $\langle\beta\rangle$ from TBW4 tend to have a positive correlation rather than anti-correlation as in BGBW fits or a lack of correlation as in default TBW. The fit parameter values are slightly different for the two TBW models as discussed below. In Fig. 5, for charged pions, kaons and protons, T from TBW4 is lower than the one in default TBW at $\sqrt{s_{\text{NN}}}$ above 62.4 GeV. For lower beam energies, within the uncertainties, T values from these two models appear to be consistent. For the cases including all hadrons and shown in Fig. 6, the results are in general with smaller uncertainties of all the fit parameters, and T from the TBW4 are lower than the default TBW for all the energies. The main observation from the comparison of BGBW and two TBW models is that T in TBW models has weaker centrality dependence and $\langle\beta\rangle$ at peripheral collisions is lower than those in BGBW.

Figure 7 shows the energy and centrality dependence of kinetic freeze-out parameters T , $\langle\beta\rangle$ and $(q-1)$ from TBW model for charged pions, kaons and protons in the left column and for all particles in the right column. The kinetic freeze-out temperature T in panel (a) and (b) of Fig. 7 shows weak collision energy dependence at $\sqrt{s_{\text{NN}}}$ of 7.7 - 39 GeV, while it drops from $\sqrt{s_{\text{NN}}} = 62.4$ GeV

to 5.02 TeV in panel (a) and 2.76 TeV in panel (b). At 7.7 - 39 GeV, at any given collision energy, T only decreases marginally from peripheral to central collisions. At 62.4 GeV to 5.02 TeV, the centrality dependence of T is even smaller. On the contrast, as discussed in previous section, in BGBW, T decreases notably from peripheral to central collisions. In most of the peripheral collisions, BGBW deviates significantly from data with larger $\chi^2/nDoF$. Meanwhile, the non-equilibrium parameter q in TBW for peripheral collisions also increases with increasing collision energy as shown in bottom two panels of Fig. 7. The strong centrality dependence of T in BGBW may be synthetic to the model's incapacity to incorporate the large non-equilibrium effect of the system in the peripheral collisions. The average transverse radial flow velocity $\langle\beta\rangle$ shown in panel (c) and (d) of Fig. 7, for most central collisions, is between 0.4 - 0.5 at RHIC energies, and around 0.6 at the LHC energies. $\langle\beta\rangle$ decreases from central to peripheral collisions. In most peripheral collisions, $\langle\beta\rangle$ drops to zero at RHIC energies and is less than 0.3 at the LHC energies. The most peripheral collisions at RHIC, the system in general fails to generate a rapid radial expansion. The non-equilibrium parameter $(q-1)$ in panel (e) and (f) of Fig. 7 is small in central Au+Au collisions, suggesting that the produced particles are approaching thermal equilibrium. In peripheral collisions, $(q-1)$ increases from less than 0.04 at 7.7 GeV to more than 0.1 at 5.02 TeV, indicating an increasing deviation from Boltzmann statistics as collision energy increases. The centrality dependence of $(q-1)$ parameter suggests an evolution from an almost thermalized system in the central collisions towards a highly off-equilibrium system in the peripheral collisions. Such large $(q-1)$ is also found in the study of $p+p$ collision [9]. This may be

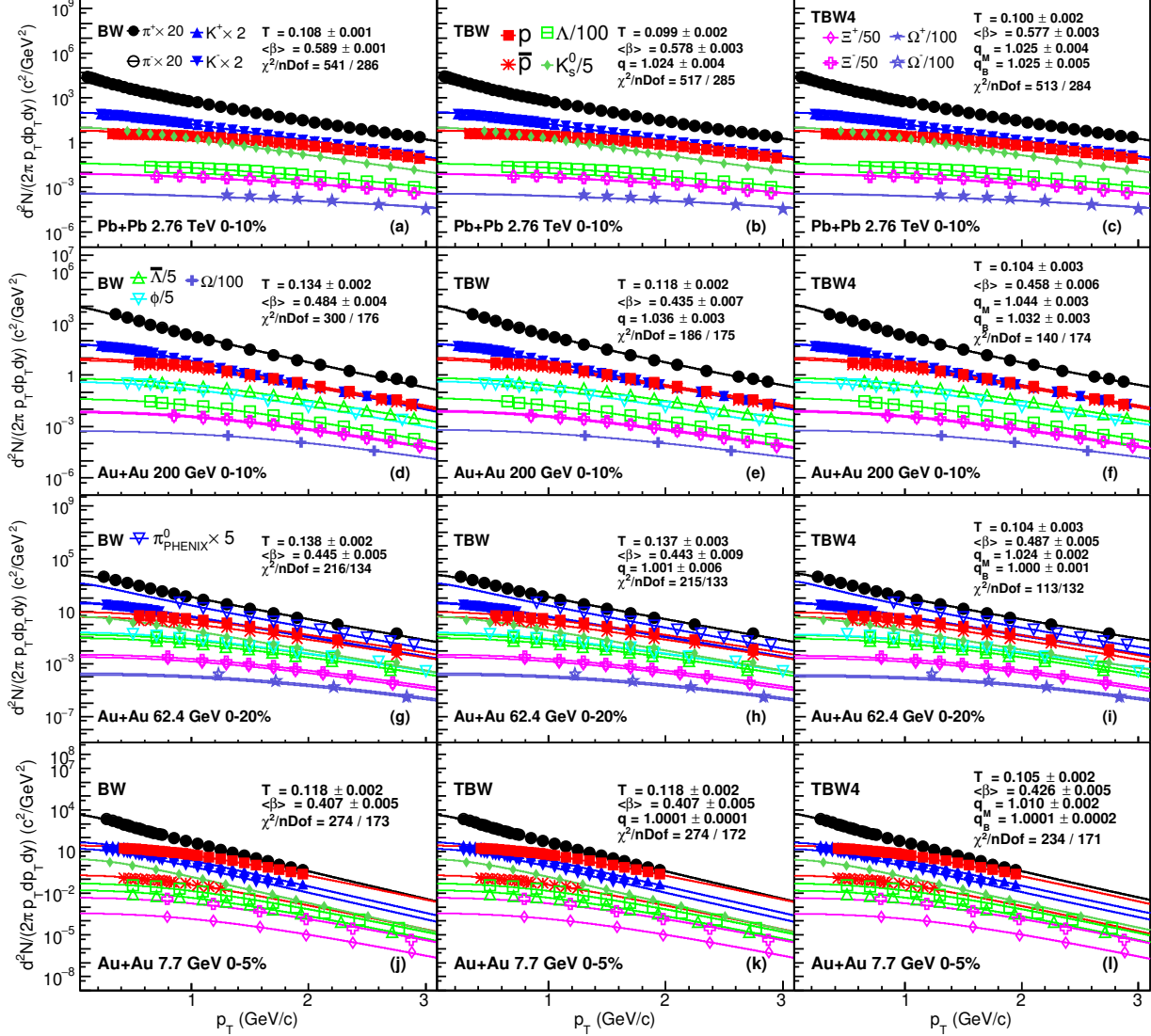


FIG. 1. Blast-wave model fits to hadron spectra in most central Pb + Pb and Au + Au collisions at $\sqrt{s_{NN}} = 2.76$ TeV, 200 GeV, 62.4 GeV and 7.7 GeV from top to bottom panels. The different symbols represent experimental data of different particle species. Uncertainties on experimental data represent quadratic sum of statistical and systematic uncertainties. The solid curves represent fit results for BGBW (left column), TBW (middle column) and TBW4 (right column).

cause that the energy density fluctuations at initial state due to Color-Glass Condensate formation or individual hard scattering (mini-jets) inside a nucleus-nucleus collision increase as collision energy increases. Such fluctuations are not completely washed out by subsequent QGP evolution or hadronic interactions and leave footprints in final state particle spectra at the p_T range in our study [21].

In general, the group of charged pion, kaon, proton and the group of all particles as shown in Fig. 7 produce similar kinetic freeze-out parameters in TBW fits. Small difference can be identified with slightly higher T and

lower q for the group with all particles than that with only the $\pi/K/p$. Such difference may come from the influence of particle species as the group of all particles contains more strange particles. The direct comparison of non-strange and strangeness in Fig. 8 confirms that the strange hadrons have higher temperature (T) and a smaller non-equilibrium degree (q) than those of non-strange hadrons, while their radial flow values ($\langle\beta\rangle$) are similar. A higher temperature indicates an earlier decoupling of strange hadrons from the system. The smaller q in the strangeness group than the non-strangeness group and a similar $\langle\beta\rangle$ between those two groups suggest that

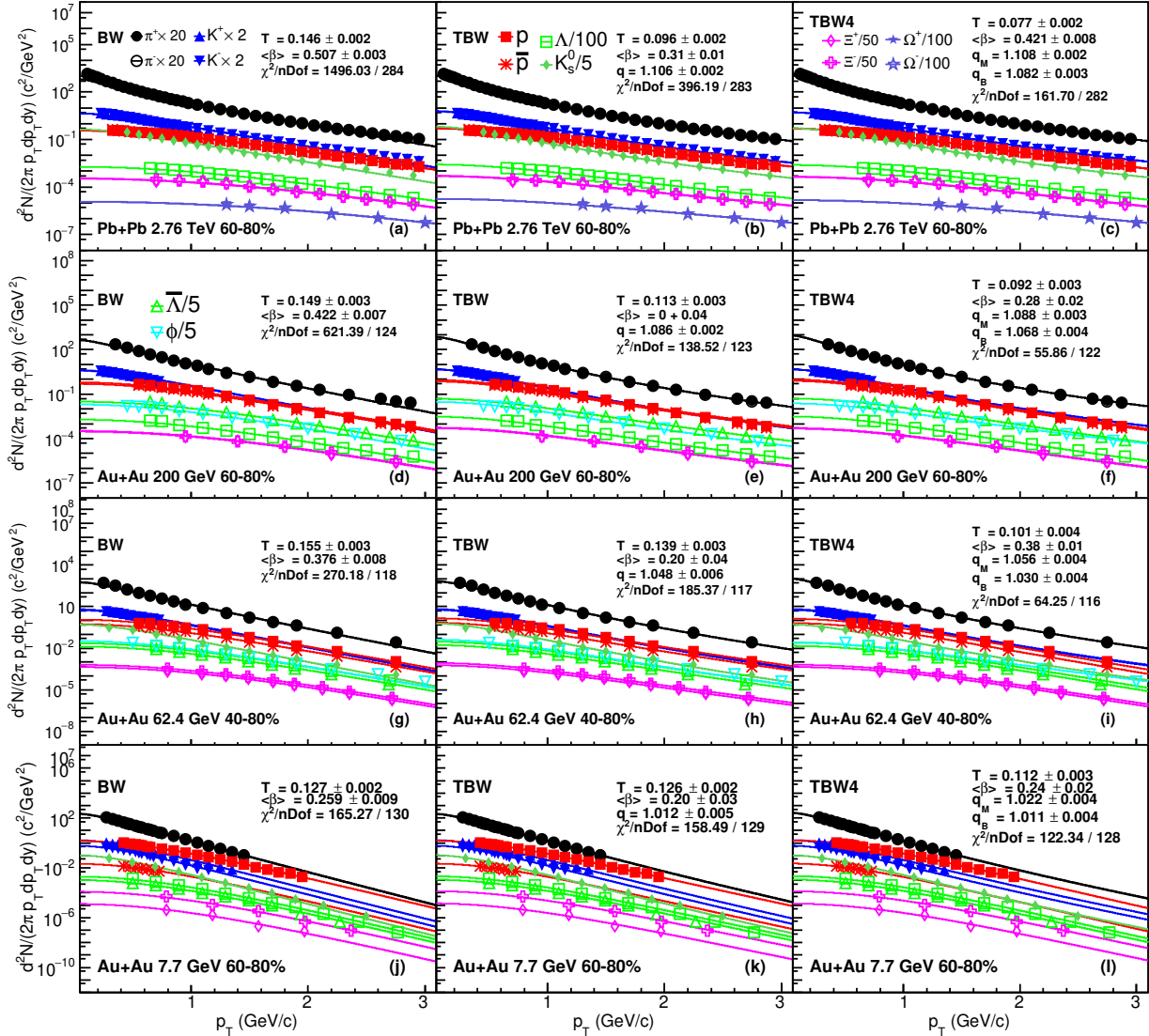


FIG. 2. Same as Fig. 1, but for most peripheral collisions.

the system is closer to an equilibrium state when the strangeness hadrons decouple from the system and further hadronic interactions do not increase the system's radial flow velocity. A possible conclusion is that the hadronic phase does not increase radial flow of light hadrons significantly at RHIC and LHC energies, instead drives the system toward non-equilibrium: the system in central collisions has approached thermal equilibrium at the partonic phase, and the later hadronic scattering drives the system off equilibrium and do not increase the radial flow of copiously produced light hadrons [22]. Another interesting observation is that in Fig. 8 (b) for non-strange particles the kinetic freeze-out temperature of the central collisions decreases from RHIC to LHC energies in TBW model, while in Fig. 8 (a) strangeness

does not show this behavior. A possible explanation is that the system at the LHC has higher flow velocity and larger volume than that at RHIC and maybe need more time for all particles to kinetic freeze-out (“cool”) in the expansion during the hadronic phase.

It has been argued within the framework of non-equilibrium statistics that the dependence of temperature and flow velocity on the non-equilibrium factor $(q - 1)$ is related to the shear and bulk ξ viscosity in linear or quadratic proportion [4, 47]. This hypothesis is examined by quadratic fits of $\langle\beta\rangle = \langle\beta\rangle_0 - a(q - 1)^2$ and $T = T_0 + b(q - 1) - d\xi(q - 1)^2$ (where ξ is the bulk viscosity) to the inclusive hadron group as shown in Figs. 9 and 10. Data at 7.7 GeV are close to equilibrium and do not provide a significant variation of the parameters,

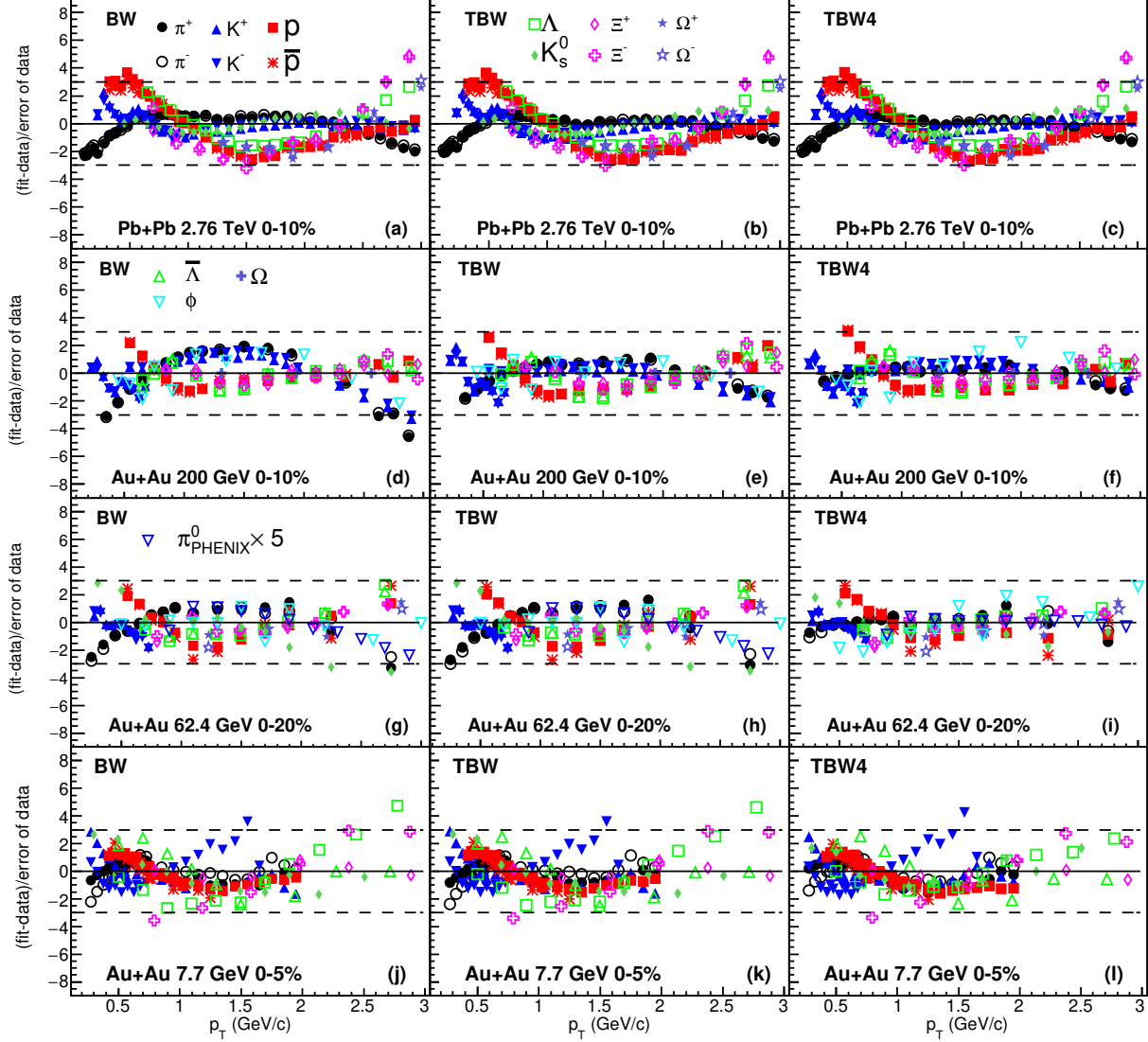


FIG. 3. The deviations of BGBW (left column), TBW (middle column) and TBW4 (right column) model fits to hadron spectra divided by data uncertainties in most central Pb + Pb and Au + Au collisions at $\sqrt{s_{NN}} = 2.76$ TeV, 200 GeV, 62.4 GeV and 7.7 GeV from top to bottom panels. The different symbols are used to distinguish particle species. The dashed lines represent where the difference between model and experiment data is 3 times the error of data.

and are not included in this examination. From 11.5 to 2.76 TeV collision energy, there displays a clear evolution of $\langle\beta\rangle$ vs $(q-1)$ and T vs $(q-1)$ relationships on collision energy. A summary of parameters $\langle\beta\rangle_0$, a , T_0 , b and $d\xi$ dependence on collision energy is depicted in Figs. 11 and 12. As energy increases, $\langle\beta\rangle_0$ increases and the coefficient of the squared term a decreases. Similar feature is observed for the T vs $(q-1)$. With only three available centrality classes, the fitting procedure at 62.4 GeV is found to be not constrained. The relationship of T vs $(q-1)$ was previously inspected in Ref. [21] for 200 GeV where only a squared term (with a constant)

is used. Our study shows that both linear or quadratic terms are needed to describe T vs $(q-1)$ relationship for lower collision energies. The linear term parameter b and quadratic term related to viscosity parameter $d\xi$ shows a trend of decrease with collision energy. It is interesting to note that it has been argued that the bulk viscosity increases dramatically toward the phase transition [48, 49], coinciding with the feature we observed of $d\xi$ shown in Fig. 12.

In a short summary, BGBW and TBW have been used to explore the beam energy dependence of kinetic freeze-out properties of the system created in relativistic heavy

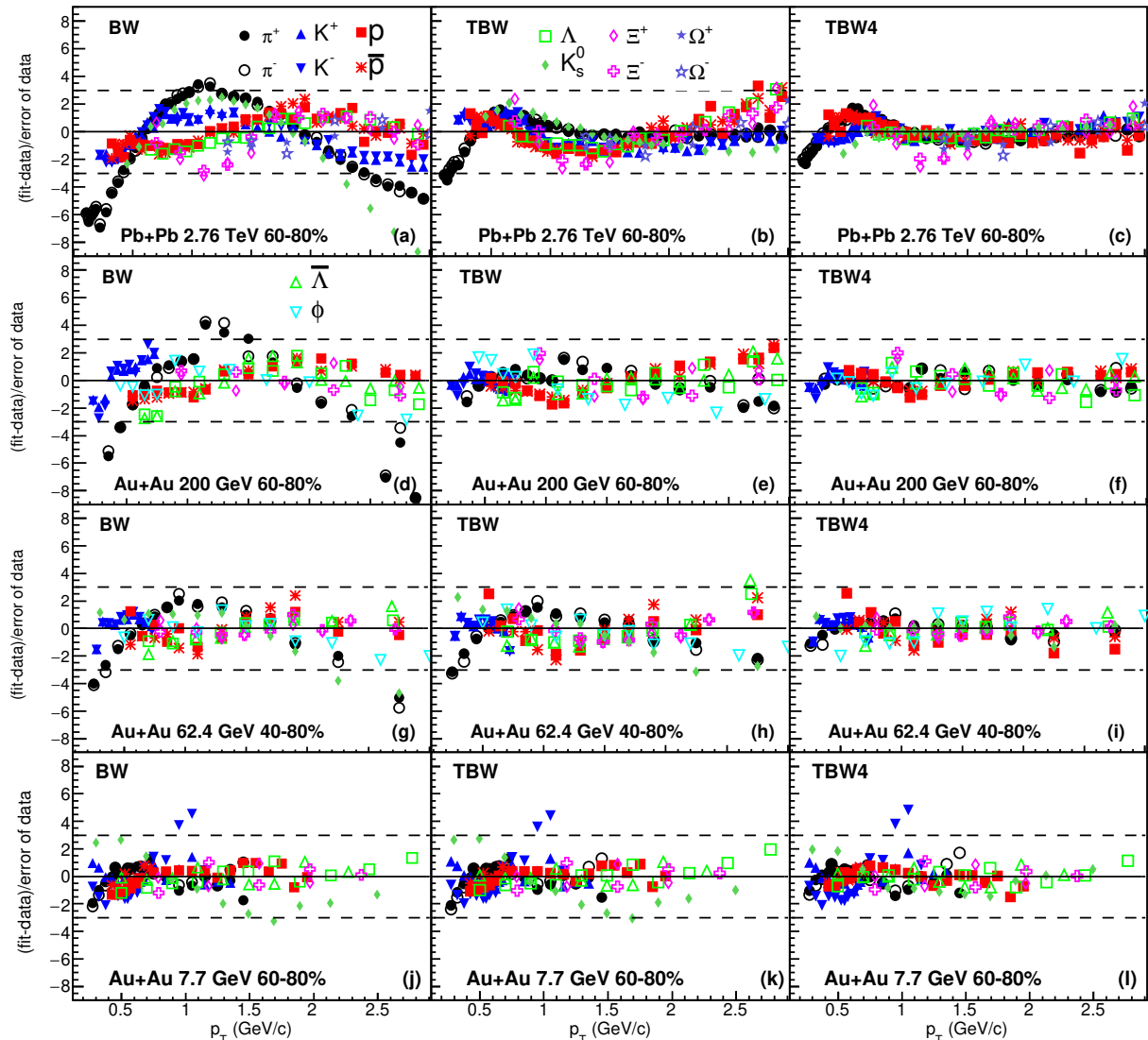


FIG. 4. Same as Fig. 3, but for most peripheral collisions.

ion collisions. BGBW model is designed to describe the system in local thermal equilibrium. However, as collision energy increases, the produced system in peripheral collisions deviates far from equilibrium state, and can not be described well with a BGBW fit. An additional parameter q is introduced in TBW model to characterize the degree of non-equilibrium. The divergence between BGBW and TBW escalates with an increasing q value as collision energy increases, especially in peripheral collisions. For 7.7 - 39 GeV collision energies, the increase of temperature in TBW model from central to peripheral collisions is much less than that in BGBW. For 62.4 GeV-5.02 TeV, the temperature in TBW model stays almost constant from central to peripheral collisions. Meanwhile, the radial flow value in central colli-

sions is around $0.4-0.5c$ at RHIC energies, and becomes larger at the LHC energies.

IV. CONCLUSION

In this work, we have used the blast-wave model with Boltzmann-Gibbs statistics and with Tsallis statistics to fit the transverse momentum spectra of hadrons produced at mid-(pseudo)rapidity in Au + Au collisions at $\sqrt{s_{NN}} = 7.7, 11.5, 14.5, 19.6, 27, 39, 62.4, 200$ GeV at RHIC and in Pb+Pb collisions at $\sqrt{s_{NN}} = 2.76$ TeV and 5.02 TeV at LHC to extract kinetic freeze-out temperature and transverse flow velocity and to study their collision centrality and energy dependence. The hadrons con-

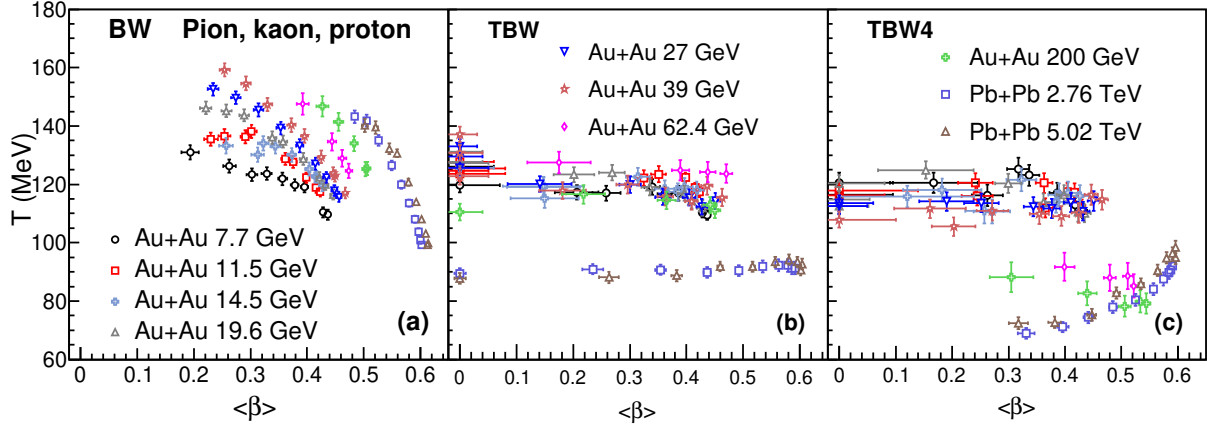


FIG. 5. Variation of T with $\langle\beta\rangle$ for different energies and centralities from BGBW (left panel), TBW (middle panel) and TBW4 (right panel) fits to p_T spectra of only positive and negative pions, kaons and protons. Symbols with same style represent different centrality classes at the same colliding energy. For a given energy, the centrality increases from left to right.

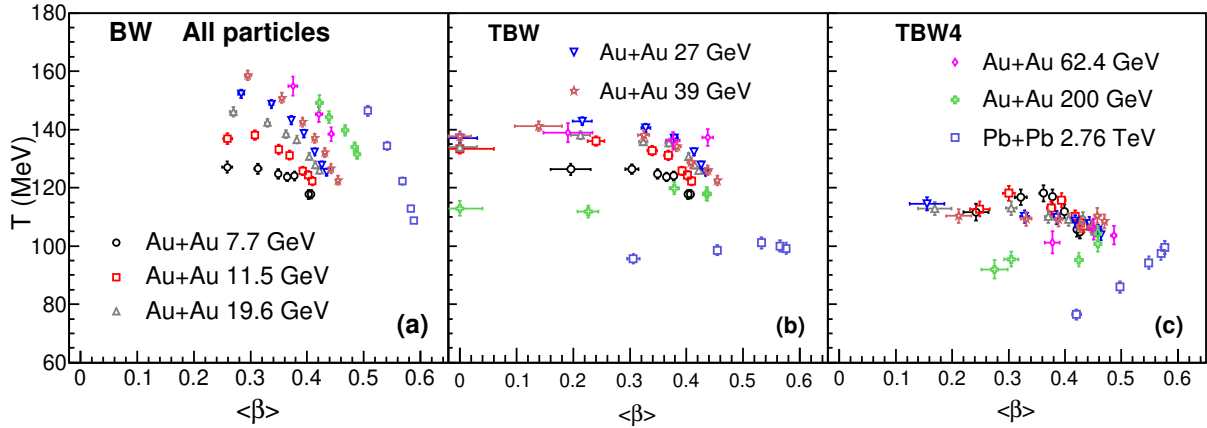


FIG. 6. Same as Fig. 5, but for all hadrons including strange and multi-strange particles.

taining strangeness at those collision energies were also examined to study their impact on the freeze-out properties. For centrality dependence, the results show that the average transverse radial flow velocity decreases and the degree of non-equilibrium q increases from central to peripheral collisions in TBW model. The kinetic freeze-out temperature shows weak dependence on centrality in TBW model, while in BGBW model there is a clear increase from central to peripheral in A + A collisions. This finding suggests that a change in non-equilibrium degree of the system in TBW is reflected as a change in freeze-out temperature in the language of transitional BGBW. One should take caution when interpreting temperature behavior in BGBW for beam energy scan results. For energy dependence in TBW fits, the average transverse

radial flow velocity and the degree of non-equilibrium q both increase with the increase of the collision energy which suggests a stronger expansion with larger deviation from thermal equilibrium at higher energy. The kinetic freeze-out temperature at the same centrality shows a weak collision energy dependence for 7.7 GeV to 39 GeV, while it decreases from 62.4 GeV to 5.02 TeV with an increase of non-equilibrium degree. A dependence of temperature and radial flow on non-equilibrium is observed and may be related to the bulk viscosity. Finally, we find that strange hadrons have a higher kinetic freeze-out temperature than that for light hadrons. The strange hadrons approach equilibrium more quickly from peripheral to central A + A collisions than non-strange hadrons.

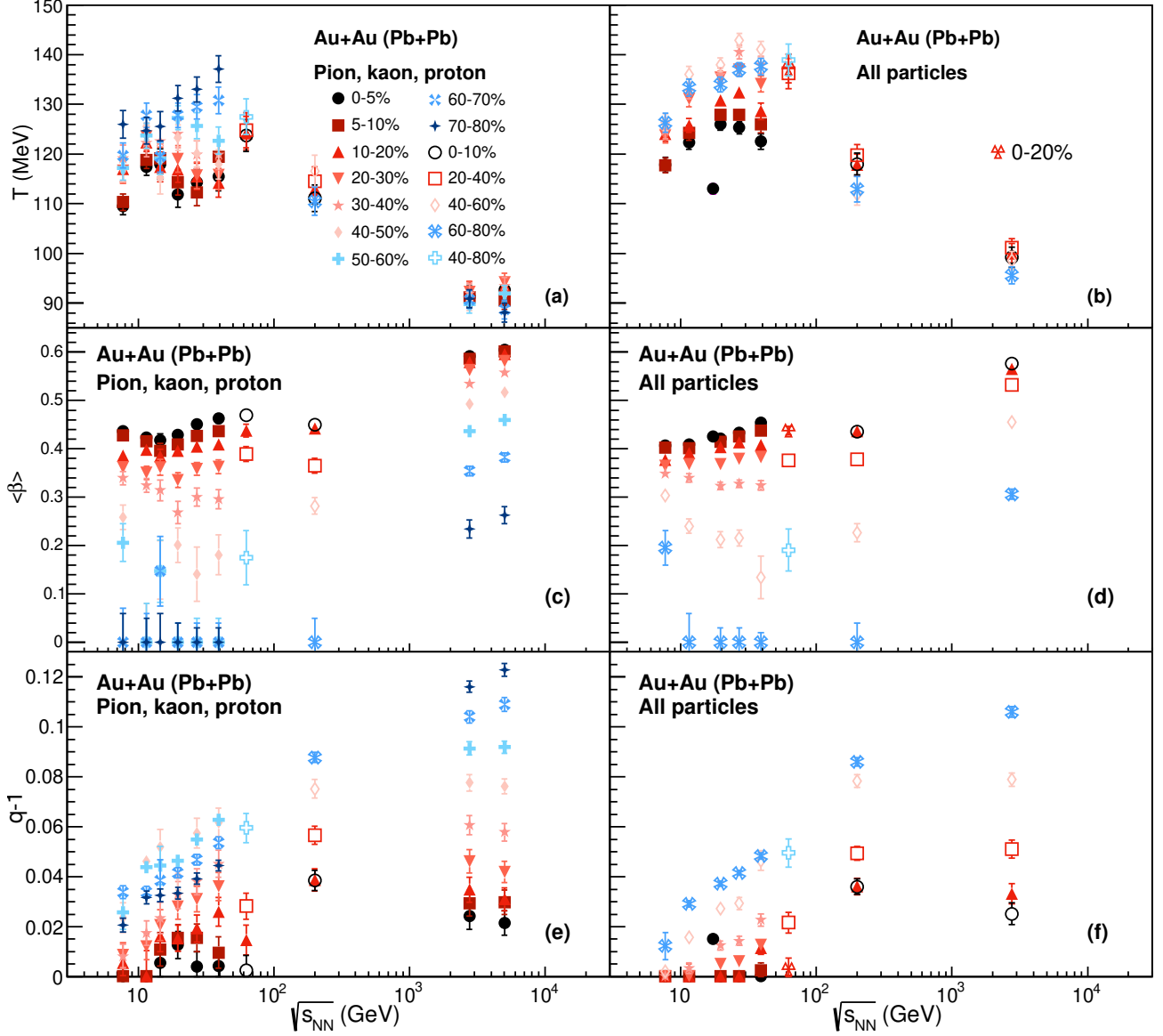


FIG. 7. Collision energy dependence of the extracted kinetic freeze-out parameters for heavy ion collisions of different centralities in TBW fit of p_T spectra for only positive and negative pions, kaons and protons (left column), and all particles (right column). The kinetic freeze-out temperature T , average transverse radial flow velocity $\langle\beta\rangle$, and non-equilibrium parameter $q - 1$ are shown in the top, middle and bottom panels, respectively. The results for all particles in most central Pb+Pb collisions at $\sqrt{s_{NN}} = 17.3$ GeV are from Ref. [22].

ACKNOWLEDGMENTS

We appreciate valuable discussion with Zhenyu Chen, Xiaofeng Luo, Nihar Ranjan Sahoo, Qinghua Xu, Chi

Yang and Qian Yang. This work was partly supported by the National Natural Science Foundation of China under Grants No.11890713 and No.11720101001. This work was also supported in part by office of science, DOE, USA.

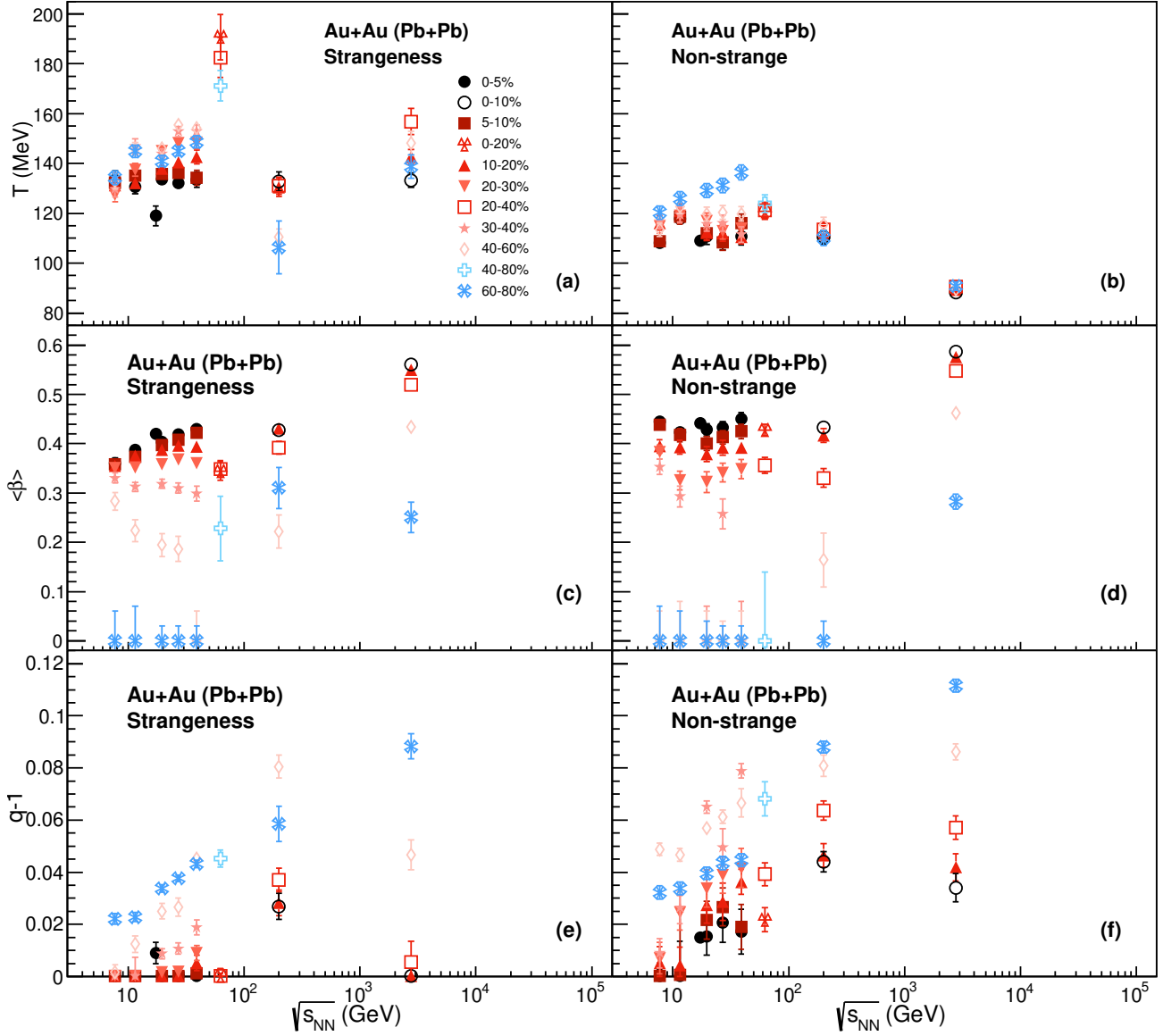


FIG. 8. Same as Fig. 7, but for strangeness only (left column), and non-strange particles (right column). The results in most central Pb+Pb collisions at $\sqrt{s_{NN}} = 17.3$ GeV are from Ref. [22].

-
- [1] E. Schnedermann, J. Sollfrank and U. W. Heinz, Phys. Rev. C **48**, 2462 (1993)
- [2] E. Schnedermann and U. W. Heinz, Phys. Rev. C **50**, 1675 (1994)
- [3] B. De, S. Bhattacharyya, G. Sau and S. K. Biswas, Int. J. Mod. Phys. E **16**, 1687 (2007).
- [4] G. Wilk and Z. Włodarczyk, Eur. Phys. J. A **40**, 299 (2009)
- [5] W. M. Alberico, A. Lavagno and P. Quarati, Eur. Phys. J. C **12**, 499 (2000)
- [6] T. Osada and G. Wilk, Phys. Rev. C **77**, 044903 (2008) Erratum: [Phys. Rev. C **78**, 069903 (2008)]
- [7] T. S. Biro and B. Muller, Phys. Lett. B **578**, 78 (2004)
- [8] T. Bhattacharyya, J. Cleymans, A. Khuntia, P. Pareek and R. Sahoo, Eur. Phys. J. A **52**, 30 (2016)
- [9] K. Jiang *et al.*, Phys. Rev. C **91**, 024910 (2015)

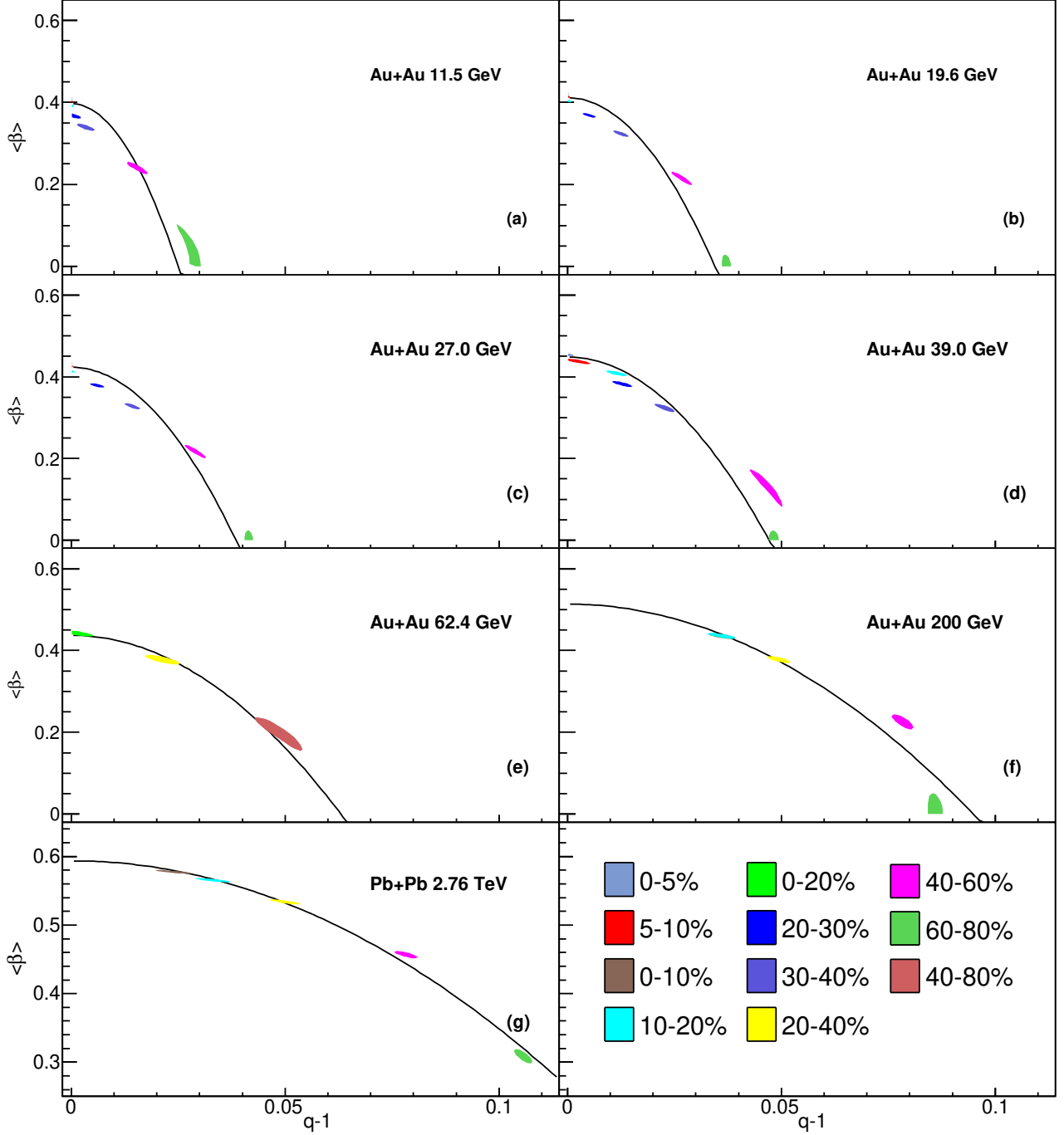


FIG. 9. Extracted average radial flow velocity $\langle\beta\rangle$ as a function of non-equilibrium degree $(q - 1)$ obtained in TBW fits of p_T spectra of all particles. Each block is one- σ contour from the error matrix of the TBW fit for a given centrality of Au + Au (Pb + Pb) collisions. The curves represent quadratics fits in the form of $\langle\beta\rangle = \langle\beta\rangle_0 - a(q - 1)^2$.

[10] K. Urmosy, G. G. Barnafoldi and T. S. Biro, Phys. Lett. B **701**, 111-116 (2011)

[11] A. Andronic, Int. J. Mod. Phys. A **29**, 1430047 (2014)

[12] B. Abelev *et al.* [ALICE Collaboration], Phys. Rev. Lett. **109**, 252301 (2012)

[13] H. L. Lao, F. H. Liu and R. A. Lacey, Eur. Phys. J. A **53**, 44 (2017) [erratum: Eur. Phys. J. A **53**, 143 (2017)]

[14] H. L. Lao, F. H. Liu, B. C. Li and M. Y. Duan, Nucl. Sci. Tech. **29**, 82 (2018)

[15] S. Zhang, Y. G. Ma, J. H. Chen and C. Zhong, Adv. High Energy Phys. **2015**, 460590 (2015)

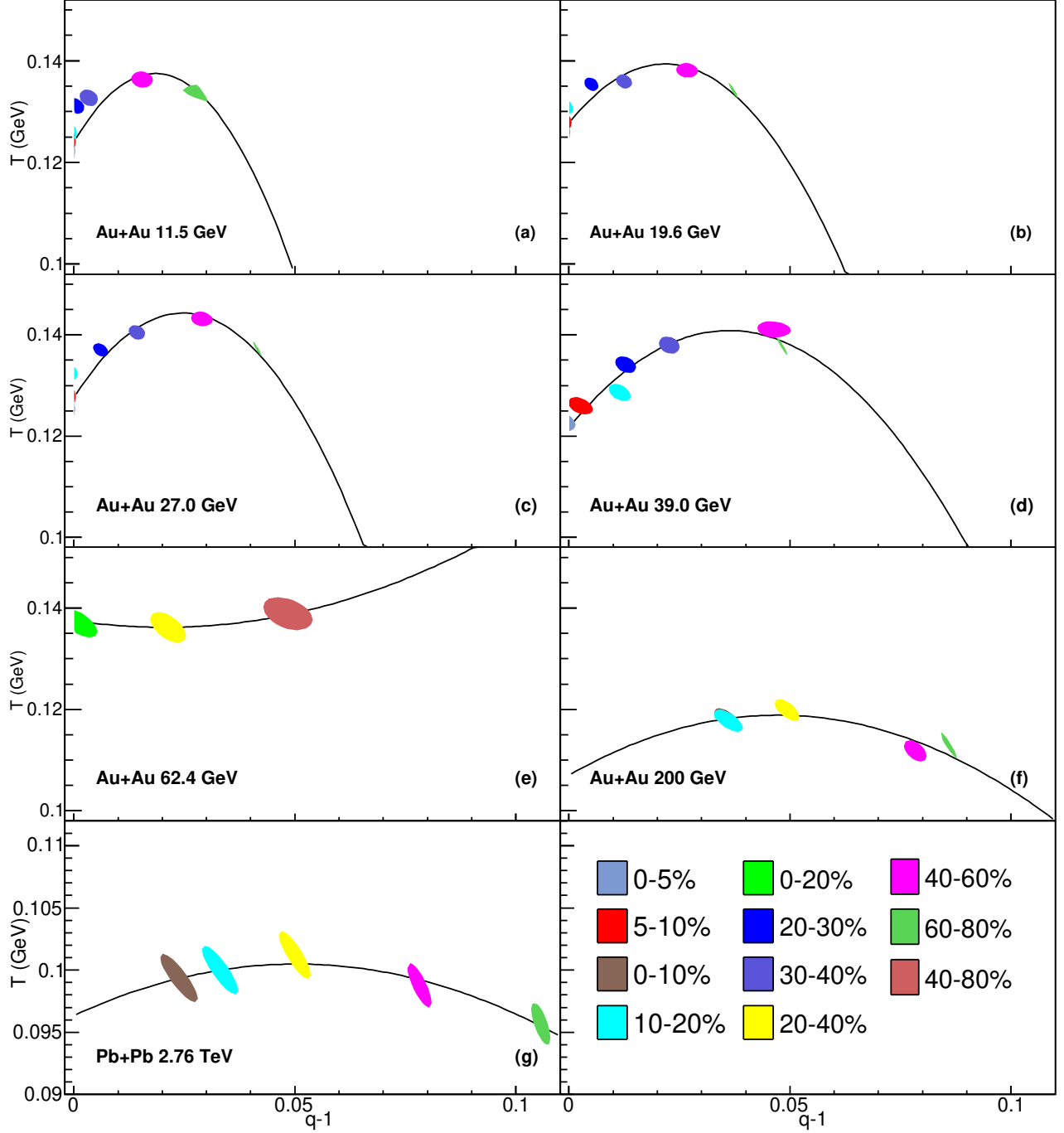


FIG. 10. Extracted kinetic freeze-out temperature T as a function of non-equilibrium degree $(q - 1)$ obtained in TBW fits of p_T spectra of all particles. Each block is one- σ contour from the error matrix of the TBW fit for a given centrality of Au + Au (Pb + Pb) collisions. The curves represent quadratics fits in the form of $T = T_0 + b(q - 1) - d\xi(q - 1)^2$.

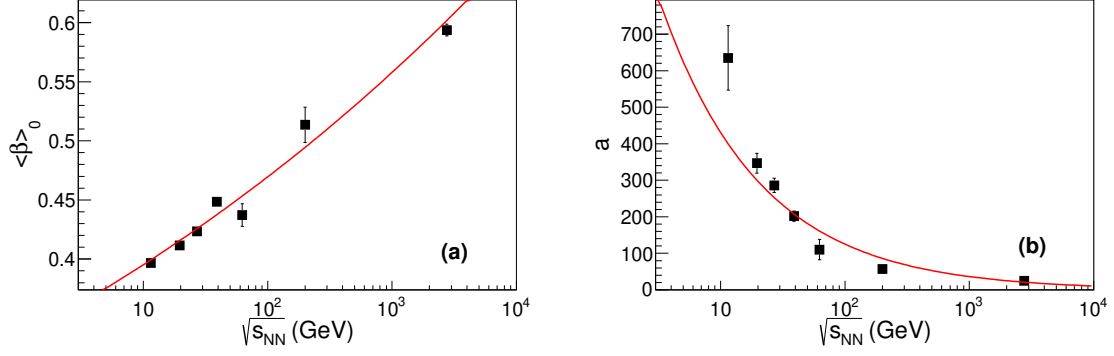
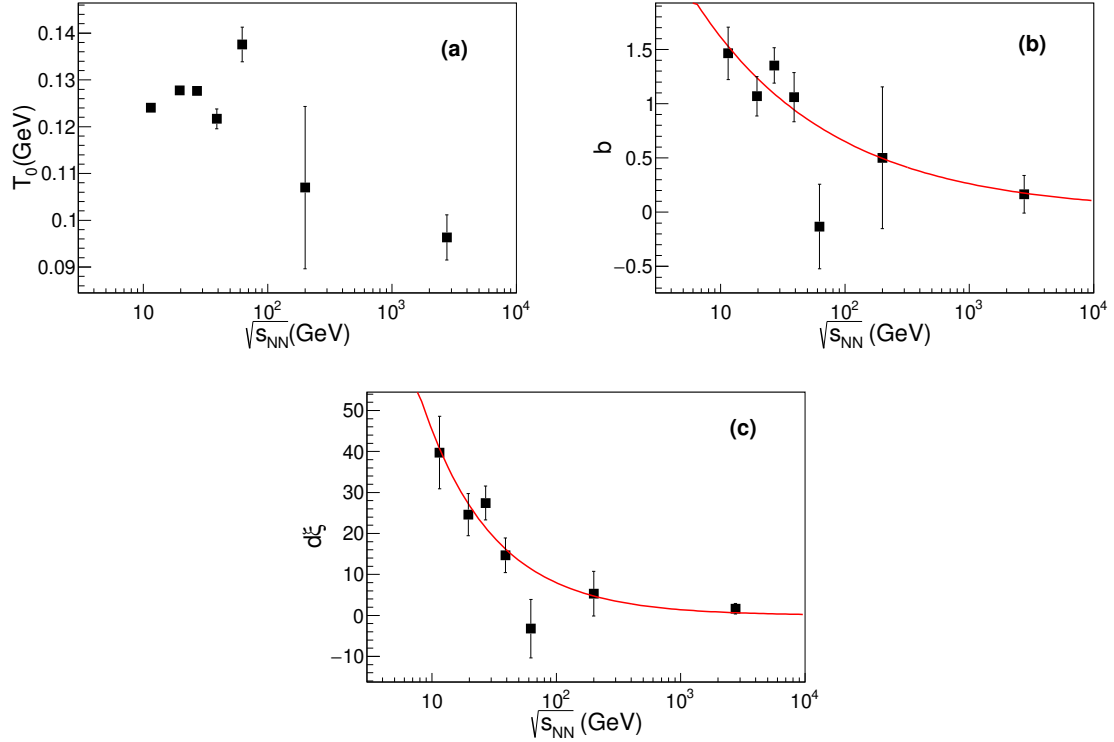
- [16] S. Zhang, Y. G. Ma, J. H. Chen and C. Zhong, Adv. High Energy Phys. **2016**, 9414239 (2016)
 [17] L. Adamczyk *et al.* [STAR Collaboration], Phys. Rev. C **96**, 044904 (2017)
 [18] S. Das [STAR Collaboration], EPJ Web Conf. **90**, 08007 (2015)

- [19] X. Luo, Nucl. Phys. A **956**, 75 (2016)
 [20] S. Chatterjee, S. Das, L. Kumar, D. Mishra, B. Mohanty, R. Sahoo and N. Sharma, Adv. High Energy Phys. **2015**, 349013 (2015).
 [21] Z. Tang, Y. Xu, L. Ruan, G. van Buren, F. Wang and Z. Xu, Phys. Rev. C **79**, 051901 (2009)

- [22] M. Shao, L. Yi, Z. Tang, H. Chen, C. Li and Z. Xu, J. Phys. G **37**, 085104 (2010)
- [23] Z. Tang *et al.*, Chin. Phys. Lett. **30**, 031201 (2013)
- [24] B. I. Abelev *et al.* [STAR Collaboration], Phys. Rev. C **79**, 034909 (2009)
- [25] B. I. Abelev *et al.* [STAR Collaboration], Phys. Rev. C **81**, 024911 (2010)
- [26] J. Adam *et al.* [STAR Collaboration], Phys. Rev. C **101**, 024905 (2020)
- [27] B. I. Abelev *et al.* [STAR Collaboration], Phys. Lett. B **655**, 104 (2007)
- [28] J. Adams *et al.* [STAR Collaboration], Phys. Rev. Lett. **92**, 112301 (2004)
- [29] B. I. Abelev *et al.* [STAR Collaboration], Phys. Rev. Lett. **97**, 152301 (2006)
- [30] B. Abelev *et al.* [ALICE Collaboration], Phys. Rev. C **88**, 044910 (2013)
- [31] S. Acharya *et al.* [ALICE], Phys. Rev. C **101**, 044907 (2020)
- [32] J. Adams *et al.* [STAR Collaboration], Nucl. Phys. A **757**, 102 (2005)
- [33] H. van Hecke, H. Sorge and N. Xu, Phys. Rev. Lett. **81**, 5764 (1998)
- [34] J. Adams *et al.* [STAR Collaboration], Phys. Rev. Lett. **92**, 182301 (2004)
- [35] M. Petrovici and A. Pop, Rom. J. Phys. **57**, 419 (2012)
- [36] O. Ristea, A. Jipa, C. Ristea, T. Esanu, M. Calin, A. Barzu, A. Scurtu and I. Abu-Quoad, J. Phys. Conf. Ser. **420**, 012041 (2013).
- [37] G. Wilk and Z. Wlodarczyk, Phys. Rev. C **79**, 054903 (2009)
- [38] J. Adam *et al.* [STAR Collaboration], Phys. Rev. C **102**, 034909 (2020)
- [39] M. M. Aggarwal *et al.* [STAR Collaboration], Phys. Rev. C **83**, 024901 (2011)
- [40] B. I. Abelev *et al.* [STAR Collaboration], Phys. Rev. C **79**, 064903 (2009)
- [41] A. Adare *et al.* [PHENIX Collaboration], Phys. Rev. Lett. **109**, 152301 (2012)
- [42] A. Adare *et al.* [PHENIX], Phys. Rev. C **88**, 024906 (2013)
- [43] J. Adams *et al.* [STAR Collaboration], Phys. Rev. Lett. **98**, 062301 (2007)
- [44] B. I. Abelev *et al.* [STAR], Phys. Rev. Lett. **99**, 112301 (2007)
- [45] B. B. Abelev *et al.* [ALICE Collaboration], Phys. Rev. Lett. **111**, 222301 (2013)
- [46] B. B. Abelev *et al.* [ALICE Collaboration], Phys. Lett. B **728**, 216 (2014) Erratum: [Phys. Lett. B **734**, 409 (2014)]
- [47] G. Wilk and Z. Wlodarczyk, Phys. Rev. Lett. **84**, 2770 (2000)
- [48] D. Kharzeev and K. Tuchin, JHEP **09**, 093 (2008)
- [49] F. Karsch, D. Kharzeev and K. Tuchin, Phys. Lett. B **663**, 217-221 (2008)

TABLE II. The fitting parameters of $\langle\beta\rangle = \langle\beta\rangle_0 - a(q-1)^2$ in Fig. 9 and $T = T_0 + b(q-1) - d\xi(q-1)^2$ in Fig. 10.

system	$\sqrt{s_{NN}}$ (GeV)	$\langle\beta\rangle_0$	a	T_0 (GeV)	b	$d\xi$
Au + Au	11.5 (all)	0.397 ± 0.002	635 ± 88	0.1240 ± 0.0009	1.5 ± 0.2	40 ± 9
Au + Au	19.6 (all)	0.411 ± 0.002	347 ± 27	0.1278 ± 0.0008	1.1 ± 0.2	25 ± 5
Au + Au	27 (all)	0.423 ± 0.002	286 ± 20	0.1277 ± 0.0008	1.4 ± 0.2	27 ± 4
Au + Au	39 (all)	0.448 ± 0.002	202 ± 14	0.122 ± 0.002	1.1 ± 0.2	15 ± 4
Au + Au	62.4 (all)	0.44 ± 0.01	110 ± 28	0.138 ± 0.004	$-(0.1 \pm 0.4)$	$-(3 \pm 7)$
Au + Au	200 (all)	0.51 ± 0.02	57 ± 6	0.11 ± 0.02	0.5 ± 0.7	5 ± 5
Pb + Pb	2760 (all)	0.594 ± 0.005	25 ± 1	0.096 ± 0.005	0.2 ± 0.2	2 ± 1

FIG. 11. Collision energy dependence of parameters $\langle\beta\rangle_0$ and a in $\langle\beta\rangle = \langle\beta\rangle_0 - a(q-1)^2$. Curves are to guide the eye.FIG. 12. Collision energy dependence of parameters T_0 , b and $d\xi$ in $T = T_0 + b(q-1) - d\xi(q-1)^2$. Curves are to guide the eye.

Appendix A

TABLE III. Extracted kinetic freeze-out parameters and $\chi^2/nDoF$ from TBW fit to identified particle transverse spectra in heavy ion collisions of different centralities at $\sqrt{s_{NN}} = 7.7$ GeV and 11.5 GeV. Results for charged pions, kaons and protons have labels ‘(π, K, p)’ behind their collision energy. All available hadrons including strange and multi-strange particles are labeled as ‘(all)’. We also fit the spectra separately for strangeness with label ‘(strange)’ and non-strange particles with label ‘(non-strange)’.

system	$\sqrt{s_{NN}}$ (GeV)	centrality	$\langle\beta\rangle$	T (MeV)	q	$\chi^2/nDoF$
Au + Au	7.7 (π, K, p)	0 – 5%	0.436 ± 0.005	110 ± 2	1.000 ± 0.002	113/133
		5 – 10%	0.428 ± 0.006	110 ± 2	1.000 ± 0.003	106/134
		10 – 20%	0.39 ± 0.01	117 ± 3	1.006 ± 0.005	86/138
		20 – 30%	0.36 ± 0.01	117 ± 3	1.009 ± 0.005	129/136
		30 – 40%	0.34 ± 0.01	119 ± 3	1.008 ± 0.005	124/135
		40 – 50%	0.26 ± 0.03	117 ± 3	1.024 ± 0.006	110/125
		50 – 60%	0.21 ± 0.04	117 ± 3	1.026 ± 0.007	132/122
		60 – 70%	$0_{-0}^{+0.07}$	120 ± 3	1.034 ± 0.003	95/117
		70 – 80%	$0_{-0}^{+0.06}$	126 ± 3	1.021 ± 0.003	88/97
		0 – 80%	0.36 ± 0.02	111 ± 3	1.019 ± 0.008	48/90
Au + Au	7.7 (non – strange)	0 – 5%	0.445 ± 0.006	108 ± 2	1.000 ± 0.003	34/89
		5 – 10%	0.438 ± 0.006	109 ± 2	1.000 ± 0.005	45/88
		10 – 20%	0.39 ± 0.01	116 ± 3	1.005 ± 0.006	37/92
		20 – 30%	0.38 ± 0.01	115 ± 3	1.007 ± 0.006	31/90
		30 – 40%	0.35 ± 0.02	117 ± 3	1.009 ± 0.006	36/90
		40 – 60%	$0_{-0}^{+0.06}$	113 ± 3	1.049 ± 0.002	52/80
		60 – 80%	$0_{-0}^{+0.07}$	120 ± 3	1.032 ± 0.003	31/62
		Au + Au	7.7 (strange)	0 – 5%	0.361 ± 0.01	133 ± 4
		5 – 10%	0.358 ± 0.01	132 ± 4	1.0001 ± 0.0002	156/82
		10 – 20%	0.356 ± 0.009	131 ± 3	1.0001 ± 0.0002	160/82
		20 – 30%	0.351 ± 0.009	128 ± 3	1.0001 ± 0.0004	160/82
		30 – 40%	0.33 ± 0.01	130 ± 3	1.000 ± 0.001	139/81
		40 – 60%	0.28 ± 0.02	133 ± 3	1.002 ± 0.003	174/75
		60 – 80%	$0_{-0}^{+0.06}$	134 ± 3	1.022 ± 0.002	119/64
Au + Au	7.7 (all)	0 – 5%	0.407 ± 0.005	118 ± 2	1.0001 ± 0.0001	274/172
		5 – 10%	0.402 ± 0.005	118 ± 2	1.0001 ± 0.0002	251/173
		10 – 20%	0.378 ± 0.005	124 ± 2	1.0001 ± 0.0002	218/177
		20 – 30%	0.365 ± 0.005	124 ± 2	1.0001 ± 0.0003	216/175
		30 – 40%	0.349 ± 0.006	125 ± 2	1.0001 ± 0.0007	189/174
		40 – 60%	0.31 ± 0.01	127 ± 2	1.002 ± 0.002	229/158
		60 – 80%	0.20 ± 0.03	126 ± 2	1.012 ± 0.005	158/129
		Au + Au	11.5 (π, K, p)	0 – 5%	0.423 ± 0.005	117 ± 2
		5 – 10%	0.416 ± 0.006	119 ± 2	1.000 ± 0.002	79/145
		10 – 20%	0.399 ± 0.006	122 ± 2	1.000 ± 0.010	92/145
		20 – 30%	0.35 ± 0.01	124 ± 3	1.012 ± 0.005	90/145
		30 – 40%	0.33 ± 0.02	122 ± 3	1.017 ± 0.005	109/144
		40 – 50%	$0_{-0}^{+0.08}$	126 ± 3	1.046 ± 0.002	114/140
		50 – 60%	$0_{-0}^{+0.08}$	124 ± 3	1.044 ± 0.002	96/138
		60 – 70%	$0_{-0}^{+0.06}$	128 ± 3	1.034 ± 0.002	108/124
		70 – 80%	$0_{-0}^{+0.05}$	125 ± 3	1.032 ± 0.003	117/120
		0 – 80%	0.37 ± 0.01	114 ± 3	1.019 ± 0.006	33/118
Au + Au	11.5 (non – strange)	0 – 5%	0.423 ± 0.005	118 ± 2	1.00 ± 0.01	63/96
		5 – 10%	0.42 ± 0.01	119 ± 3	1.00 ± 0.03	49/97
		10 – 20%	0.39 ± 0.01	121 ± 3	1.004 ± 0.007	68/97
		20 – 30%	0.33 ± 0.02	119 ± 3	1.025 ± 0.007	56/97
		30 – 40%	0.29 ± 0.02	120 ± 3	1.026 ± 0.006	56/97
		40 – 60%	$0_{-0}^{+0.08}$	123 ± 3	1.047 ± 0.002	61/92
		60 – 80%	$0_{-0}^{+0.06}$	126 ± 3	1.034 ± 0.002	65/82
		0 – 80%	0.37 ± 0.02	113 ± 3	1.021 ± 0.008	21/82

TABLE IV. Same as Table III, but for $\sqrt{s_{NN}} = 11.5$ GeV (continued), 14.5 GeV, 17.3 GeV, and 19.6 GeV. The results at $\sqrt{s_{NN}} = 17.3$ GeV are from Ref. [22].

system	$\sqrt{s_{NN}}$ (GeV)	centrality	$\langle\beta\rangle$	T (MeV)	q	$\chi^2/nDoF$
Au + Au	11.5 (strange)	0 – 5%	0.387 ± 0.007	131 ± 3	1.0001 ± 0.0002	148/84
		5 – 10%	0.373 ± 0.008	135 ± 3	1.0001 ± 0.0004	154/86
		10 – 20%	0.376 ± 0.007	132 ± 2	1.0001 ± 0.0005	134/86
		20 – 30%	0.352 ± 0.007	138 ± 3	1.000 ± 0.001	107/86
		30 – 40%	0.313 ± 0.009	147 ± 3	1.000 ± 0.007	92/85
		40 – 60%	0.22 ± 0.02	146 ± 3	1.012 ± 0.003	126/84
		60 – 80%	$0_{-0}^{+0.07}$	145 ± 3	1.023 ± 0.002	132/73
Au + Au	11.5 (all)	0 – 5%	0.409 ± 0.004	122 ± 1	1.0001 ± 0.0002	228/183
		5 – 10%	0.402 ± 0.004	124 ± 2	1.0001 ± 0.0003	227/186
		10 – 20%	0.392 ± 0.004	126 ± 1	1.0001 ± 0.0006	214/186
		20 – 30%	0.368 ± 0.007	131 ± 2	1.000 ± 0.005	185/186
		30 – 40%	0.340 ± 0.009	133 ± 2	1.003 ± 0.002	205/185
		40 – 60%	0.24 ± 0.01	136 ± 2	1.015 ± 0.002	228/179
		60 – 80%	$0_{-0}^{+0.06}$	134 ± 2	1.029 ± 0.001	240/158
Au + Au	14.5 (π, K, p)	0 – 5%	0.42 ± 0.01	118 ± 3	1.006 ± 0.007	56/149
		5 – 10%	0.40 ± 0.01	119 ± 3	1.011 ± 0.007	58/149
		10 – 20%	0.38 ± 0.02	117 ± 3	1.016 ± 0.006	53/149
		20 – 30%	0.36 ± 0.02	118 ± 3	1.021 ± 0.006	33/149
		30 – 40%	0.31 ± 0.02	123 ± 3	1.024 ± 0.006	57/149
		40 – 50%	0.15 ± 0.06	115 ± 3	1.052 ± 0.007	83/143
		50 – 60%	0.15 ± 0.06	119 ± 3	1.045 ± 0.008	110/139
		60 – 70%	0.15 ± 0.07	119 ± 3	1.039 ± 0.008	79/131
		70 – 80%	$0_{-0}^{+0.06}$	126 ± 3	1.033 ± 0.003	93/127
Pb + Pb	17.3 (non-strange) [22]	0 – 5%	0.442 ± 0.005	109 ± 1	1.015 ± 0.001	102/86
Pb + Pb	17.3 (strange) [22]	0 – 5%	0.420 ± 0.007	119 ± 4	1.009 ± 0.004	137/70
Pb + Pb	17.3 (all) [22]	0 – 5%	0.426 ± 0.004	113 ± 1	1.015 ± 0.001	267/159
Au + Au	19.6 (π, K, p)	0 – 5%	0.428 ± 0.009	112 ± 3	1.013 ± 0.005	52/146
		5 – 10%	0.41 ± 0.01	114 ± 3	1.016 ± 0.005	155/142
		10 – 20%	0.40 ± 0.01	117 ± 3	1.015 ± 0.005	73/142
		20 – 30%	0.34 ± 0.02	119 ± 3	1.028 ± 0.005	71/142
		30 – 40%	0.27 ± 0.02	124 ± 3	1.033 ± 0.006	84/143
		40 – 50%	0.20 ± 0.04	123 ± 3	1.041 ± 0.006	88/141
		50 – 60%	$0_{-0}^{+0.05}$	127 ± 2	1.047 ± 0.002	128/141
		60 – 70%	$0_{-0}^{+0.04}$	128 ± 3	1.042 ± 0.002	192/135
		70 – 80%	$0_{-0}^{+0.04}$	131 ± 3	1.033 ± 0.002	234/130
		0 – 80%	0.35 ± 0.01	111 ± 3	1.036 ± 0.006	33/127
Au + Au	19.6 (non – strange)	0 – 5%	0.43 ± 0.01	111 ± 3	1.015 ± 0.007	40/96
		5 – 10%	0.40 ± 0.01	112 ± 3	1.022 ± 0.007	53/92
		10 – 20%	0.38 ± 0.02	112 ± 3	1.027 ± 0.007	36/92
		20 – 30%	0.32 ± 0.02	117 ± 3	1.034 ± 0.007	53/92
		30 – 40%	$0_{-0}^{+0.07}$	116 ± 3	1.065 ± 0.002	68/93
		40 – 60%	$0_{-0}^{+0.06}$	120 ± 3	1.057 ± 0.002	48/93
		60 – 80%	$0_{-0}^{+0.04}$	129 ± 3	1.040 ± 0.002	125/88
		0 – 80%	0.34 ± 0.02	110 ± 3	1.038 ± 0.007	24/86
Au + Au	19.6 (strange)	0 – 5%	0.404 ± 0.004	134 ± 2	1.0001 ± 0.0001	201/88
		5 – 10%	0.397 ± 0.004	136 ± 2	1.0001 ± 0.0003	181/88
		10 – 20%	0.388 ± 0.004	138 ± 2	1.0001 ± 0.0004	188/88
		20 – 30%	0.359 ± 0.007	145 ± 2	1.002 ± 0.002	182/88
		30 – 40%	0.319 ± 0.009	144 ± 2	1.009 ± 0.002	224/88
		40 – 60%	0.19 ± 0.02	146 ± 2	1.025 ± 0.003	271/86
		60 – 80%	$0_{-0}^{+0.03}$	141 ± 2	1.034 ± 0.001	265/79

TABLE V. Same as Table III, but for $\sqrt{s_{NN}} = 19.6$ GeV (continued), 27 GeV and 39 GeV.

system	$\sqrt{s_{NN}}$ (GeV)	centrality	$\langle\beta\rangle$	T (MeV)	q	$\chi^2/nDoF$
Au + Au	19.6 (all)	0 – 5%	0.421 ± 0.003	126 ± 1	1.0001 ± 0.0002	293/187
		5 – 10%	0.414 ± 0.003	128 ± 1	1.0001 ± 0.0005	282/183
		10 – 20%	0.404 ± 0.003	131 ± 1	1.000 ± 0.001	278/183
		20 – 30%	0.369 ± 0.006	135 ± 1	1.005 ± 0.002	312/183
		30 – 40%	0.324 ± 0.008	136 ± 1	1.013 ± 0.002	343/184
		40 – 60%	0.22 ± 0.02	138 ± 1	1.027 ± 0.002	374/182
		60 – 80%	$0_{-0}^{+0.03}$	134 ± 2	1.037 ± 0.001	411/170
		Au + Au	27 (π, K, p)	0 – 5%	0.451 ± 0.009	114 ± 3
5 – 10%	0.43 ± 0.01			112 ± 3	1.016 ± 0.006	66/140
10 – 20%	0.40 ± 0.01			116 ± 3	1.019 ± 0.005	61/140
20 – 30%	0.36 ± 0.01			116 ± 3	1.031 ± 0.005	54/140
30 – 40%	0.30 ± 0.02			120 ± 3	1.038 ± 0.005	57/140
40 – 50%	0.14 ± 0.06			120 ± 3	1.058 ± 0.006	48/140
50 – 60%	$0_{-0}^{+0.05}$			126 ± 3	1.055 ± 0.002	102/140
60 – 70%	$0_{-0}^{+0.04}$			130 ± 3	1.047 ± 0.002	162/140
70 – 80%	$0_{-0}^{+0.03}$			133 ± 3	1.039 ± 0.002	267/138
0 – 80%	0.38 ± 0.01			115 ± 3	1.027 ± 0.005	49/137
Au + Au	27 (non – strange)	0 – 5%	0.43 ± 0.01	109 ± 3	1.021 ± 0.008	38/90
		5 – 10%	0.41 ± 0.01	108 ± 3	1.027 ± 0.007	39/90
		10 – 20%	0.39 ± 0.02	112 ± 3	1.029 ± 0.007	32/90
		20 – 30%	0.34 ± 0.02	113 ± 3	1.039 ± 0.007	29/90
		30 – 40%	0.26 ± 0.03	116 ± 3	1.050 ± 0.007	31/90
		40 – 60%	$0_{-0}^{+0.04}$	120 ± 3	1.061 ± 0.003	38/90
		60 – 80%	$0_{-0}^{+0.03}$	131 ± 3	1.044 ± 0.003	125/88
		0 – 80%	0.36 ± 0.02	110 ± 3	1.039 ± 0.007	22/88
Au + Au	27 (strange)	0 – 5%	0.419 ± 0.004	132 ± 2	1.0001 ± 0.0002	263/87
		5 – 10%	0.408 ± 0.004	136 ± 2	1.0001 ± 0.0002	199/88
		10 – 20%	0.396 ± 0.004	141 ± 2	1.0001 ± 0.0004	189/88
		20 – 30%	0.368 ± 0.006	148 ± 2	1.002 ± 0.002	177/88
		30 – 40%	0.31 ± 0.01	153 ± 2	1.011 ± 0.002	154/88
		40 – 60%	0.19 ± 0.03	155 ± 2	1.027 ± 0.003	201/88
		60 – 80%	$0_{-0}^{+0.03}$	145 ± 2	1.038 ± 0.001	253/88
		Au + Au	27 (all)	0 – 5%	0.434 ± 0.003	125 ± 1
5 – 10%	0.426 ± 0.003			128 ± 1	1.0001 ± 0.0003	302/181
10 – 20%	0.414 ± 0.003			132 ± 1	1.0001 ± 0.0009	290/181
20 – 30%	0.379 ± 0.005			137 ± 1	1.006 ± 0.002	316/181
30 – 40%	0.328 ± 0.008			141 ± 1	1.014 ± 0.002	302/181
40 – 60%	0.22 ± 0.02			143 ± 1	1.029 ± 0.003	348/181
60 – 80%	$0_{-0}^{+0.03}$			137 ± 1	1.042 ± 0.001	422/179
Au + Au	39 (π, K, p)			0 – 5%	0.463 ± 0.009	116 ± 3
		5 – 10%	0.44 ± 0.01	120 ± 3	1.010 ± 0.006	61/140
		10 – 20%	0.41 ± 0.01	114 ± 3	1.026 ± 0.006	48/140
		20 – 30%	0.36 ± 0.01	116 ± 3	1.036 ± 0.006	63/140
		30 – 40%	0.30 ± 0.02	120 ± 3	1.045 ± 0.006	53/140
		40 – 50%	0.18 ± 0.04	118 ± 3	1.062 ± 0.006	55/140
		50 – 60%	$0_{-0}^{+0.05}$	123 ± 3	1.063 ± 0.002	94/140
		60 – 70%	$0_{-0}^{+0.04}$	131 ± 3	1.054 ± 0.002	226/140
		70 – 80%	$0_{-0}^{+0.03}$	137 ± 3	1.045 ± 0.002	341/140
		0 – 80%	0.38 ± 0.01	117 ± 3	1.030 ± 0.006	46/140

TABLE VI. Same as Table III, but for $\sqrt{s_{NN}} = 39$ GeV (continued), 62.4 GeV and 200 GeV.

system	$\sqrt{s_{NN}}$ (GeV)	centrality	$\langle\beta\rangle$	T (MeV)	q	$\chi^2/nDoF$
Au + Au	39 (non – strange)	0 – 5% ^a	0.45 ± 0.01	111 ± 4	1.017 ± 0.009	39/90
		5 – 10% ^a	0.43 ± 0.01	116 ± 4	1.019 ± 0.009	45/90
		10 – 20%	0.39 ± 0.01	111 ± 3	1.036 ± 0.005	40/100
		20 – 30% ^a	0.35 ± 0.02	114 ± 4	1.042 ± 0.008	50/90
		30 – 40% ^a	$0_{-0}^{+0.08}$	112 ± 3	1.079 ± 0.003	49/90
		40 – 60%	$0_{-0}^{+0.06}$	120 ± 3	1.067 ± 0.005	43/100
		60 – 80% ^a	$0_{-0}^{+0.03}$	137 ± 3	1.045 ± 0.003	158/90
		0 – 80% ^a	0.37 ± 0.02	114 ± 3	1.039 ± 0.008	35/90
Au + Au	39 (strange)	0 – 5%	0.430 ± 0.007	134 ± 3	1.000 ± 0.003	65/88
		5 – 10%	0.42 ± 0.01	134 ± 3	1.001 ± 0.003	73/88
		10 – 20%	0.39 ± 0.01	143 ± 3	1.005 ± 0.003	85/88
		20 – 30%	0.36 ± 0.01	148 ± 3	1.009 ± 0.003	110/88
		30 – 40%	0.30 ± 0.02	153 ± 3	1.019 ± 0.003	93/88
		40 – 60%	$0_{-0}^{+0.06}$	154 ± 2	1.045 ± 0.001	166/88
		60 – 80%	$0_{-0}^{+0.03}$	149 ± 2	1.043 ± 0.002	221/88
		0 – 80%				
Au + Au	39 (all)	0 – 5% ^a	0.454 ± 0.004	123 ± 2	1.000 ± 0.002	131/181
		5 – 10% ^a	0.438 ± 0.007	126 ± 2	1.003 ± 0.003	133/181
		10 – 20%	0.408 ± 0.007	129 ± 2	1.012 ± 0.003	190/191
		20 – 30% ^a	0.382 ± 0.008	134 ± 2	1.013 ± 0.002	234/181
		30 – 40% ^a	0.32 ± 0.01	138 ± 2	1.023 ± 0.002	214/181
		40 – 60%	0.14 ± 0.04	141 ± 2	1.046 ± 0.004	309/191
		60 – 80% ^a	$0_{-0}^{+0.02}$	138 ± 2	1.048 ± 0.001	464/181
		0 – 80%				
Au + Au	62.4 (π, K, p)	0 – 10%	0.47 ± 0.01	124 ± 3	1.002 ± 0.006	104/65
		10 – 20%	0.44 ± 0.01	124 ± 3	1.015 ± 0.006	96/65
		20 – 40%	0.39 ± 0.02	125 ± 4	1.028 ± 0.005	85/65
		40 – 80%	0.18 ± 0.05	128 ± 4	1.059 ± 0.006	91/65
Au + Au	62.4 (non – strange)	0 – 20%	0.43 ± 0.01	121 ± 3	1.022 ± 0.005	93/57
		20 – 40%	0.36 ± 0.02	121 ± 3	1.039 ± 0.004	69/57
		40 – 80% ^a	$0_{-0}^{+0.14}$	124 ± 4	1.068 ± 0.007	73/47
Au + Au	62.4 (strange)	0 – 20%	0.34 ± 0.02	190 ± 10	1.000 ± 0.001	50/73
		20 – 40%	0.35 ± 0.02	182 ± 8	1.000 ± 0.003	43/73
		40 – 80%	0.23 ± 0.07	169 ± 7	1.03 ± 0.01	70/67
Au + Au	62.4 (all)	0 – 20%	0.443 ± 0.009	137 ± 3	1.001 ± 0.006	215/133
		20 – 40%	0.38 ± 0.01	136 ± 3	1.021 ± 0.004	181/133
		40 – 80% ^a	0.20 ± 0.04	139 ± 3	1.048 ± 0.006	185/117
Au + Au	200 (π, K, p)	0 – 10% ^b	0.45 ± 0.01	111 ± 3	1.039 ± 0.004	105/79
		10 – 20%	0.44 ± 0.01	113 ± 3	1.039 ± 0.005	98/79
		20 – 40%	0.36 ± 0.02	115 ± 3	1.057 ± 0.004	112/81
		40 – 60%	0.22 ± 0.04	117 ± 3	1.075 ± 0.004	87/81
		60 – 80%	$0_{-0}^{+0.04}$	111 ± 3	1.088 ± 0.002	79/81
Au + Au	200 (non – strange)	0 – 10% ^b	0.43 ± 0.01	110 ± 3	1.044 ± 0.004	73/61
		10 – 20%	0.42 ± 0.01	112 ± 3	1.047 ± 0.005	67/59
		20 – 40%	0.33 ± 0.02	114 ± 3	1.064 ± 0.004	75/61
		40 – 60%	0.16 ± 0.05	115 ± 3	1.081 ± 0.004	68/61
		60 – 80%	$0_{-0}^{+0.04}$	110 ± 3	1.088 ± 0.002	74/61
Au + Au	200 (strange)	0 – 10% ^c	0.43 ± 0.01	133 ± 4	1.027 ± 0.005	92/111
		10 – 20% ^d	0.43 ± 0.01	131 ± 4	1.028 ± 0.005	112/111
		20 – 40%	0.39 ± 0.01	131 ± 3	1.037 ± 0.005	171/113
		40 – 60%	0.22 ± 0.03	110 ± 3	1.081 ± 0.004	165/113
		60 – 80% ^e	0.31 ± 0.04	110 ± 10	1.059 ± 0.007	54/59

^a Lack of measurements of π^0 at this centrality class [41].^b The measurements of π^\pm , p and \bar{p} for centrality 0-12% [29] are used as 0-10%.^c The measurements of Λ , $\bar{\Lambda}$, Ξ^+ , Ξ^- and Ω for centrality 0-5% [43] are used as 0-10%.^d Lack of measurements of Ω at this centrality class [43].^e Lack of measurements of Ω [43] and intermediate p_T K^\pm [42] at this centrality class.

TABLE VII. Same as Table III, but for $\sqrt{s_{\text{NN}}} = 200$ GeV (continued), 2760 GeV and 5020 GeV. Previous studies of 200 GeV from Refs. [21, 22] are also listed. The difference between our results at 200 GeV from previous ones is because that more data points at $2 \text{ GeV}/c \leq p_T \leq 3 \text{ GeV}/c$ are available now and are thus used in fitting, mainly K^\pm from PHENIX [42] which provides better constraint on q , while data for K^\pm used in Ref. [21] is only at $p_T \leq 0.8 \text{ GeV}/c$ and data for K^\pm used in Ref.[22] is only at $p_T \leq 2 \text{ GeV}/c$.

system	$\sqrt{s_{\text{NN}}}$ (GeV)	centrality	$\langle\beta\rangle$	T (MeV)	q	$\chi^2/nDoF$		
Au + Au	200 (all)	0 – 10% ^a	0.435 ± 0.007	118 ± 2	1.036 ± 0.003	186/175		
		10 – 20% ^b	0.436 ± 0.007	118 ± 2	1.036 ± 0.003	198/173		
		20 – 40%	0.378 ± 0.009	120 ± 2	1.049 ± 0.003	278/177		
		40 – 60%	0.23 ± 0.02	112 ± 2	1.078 ± 0.003	237/177		
		60 – 80% ^c	$0_{-0}^{+0.04}$	113 ± 3	1.086 ± 0.002	139/123		
Au + Au	200 (all) [21]	0 – 10%	0.470 ± 0.009	122 ± 2	1.018 ± 0.005	130/125		
		10 – 20%	0.475 ± 0.008	122 ± 2	1.015 ± 0.005	119/127		
		20 – 40%	0.441 ± 0.009	124 ± 2	1.024 ± 0.004	159/127		
		40 – 60%	0.282 ± 0.017	119 ± 2	1.066 ± 0.003	165/135		
		60 – 80%	$0_{-0}^{+0.05}$	114 ± 3	1.086 ± 0.002	138/123		
Au + Au	200 (all) [22]	0 – 10%	0.472 ± 0.009	122 ± 3	1.017 ± 0.006	140/155		
Pb + Pb	2760 (π, K, p)	0 – 5%	0.591 ± 0.003	91 ± 2	1.024 ± 0.005	247/213		
		5 – 10%	0.587 ± 0.003	91 ± 2	1.029 ± 0.005	247/213		
		10 – 20%	0.580 ± 0.003	92 ± 2	1.035 ± 0.005	230/213		
		20 – 30%	0.563 ± 0.004	92 ± 2	1.046 ± 0.005	207/213		
		30 – 40%	0.535 ± 0.005	92 ± 2	1.061 ± 0.004	201/213		
		40 – 50%	0.493 ± 0.005	90 ± 2	1.078 ± 0.003	185/213		
		50 – 60%	0.437 ± 0.007	90 ± 2	1.091 ± 0.003	196/213		
		60 – 70%	0.35 ± 0.01	91 ± 2	1.104 ± 0.002	244/213		
		70 – 80%	0.23 ± 0.02	91 ± 2	1.116 ± 0.002	299/213		
Pb + Pb	2760 (non – strange)	80 – 90%	$0_{-0}^{+0.01}$	90 ± 2	1.122 ± 0.001	344/213		
		0 – 10%	0.587 ± 0.003	88 ± 2	1.034 ± 0.005	209/143		
		10 – 20%	0.576 ± 0.004	89 ± 2	1.042 ± 0.005	201/143		
		20 – 40%	0.548 ± 0.005	91 ± 2	1.057 ± 0.005	189/143		
		40 – 60%	0.463 ± 0.007	90 ± 2	1.086 ± 0.003	168/143		
		60 – 80%	0.28 ± 0.01	91 ± 2	1.112 ± 0.003	198/143		
		80 – 90%	$0_{-0}^{+0.01}$	90 ± 2	1.120 ± 0.001	225/143		
		Pb + Pb	2760 (strange)	0 – 10%	0.561 ± 0.003	133 ± 3	1.000 ± 0.001	125/139
				10 – 20%	0.550 ± 0.003	143 ± 3	1.000 ± 0.002	74/139
20 – 40%	0.519 ± 0.008			157 ± 5	1.006 ± 0.008	61/139		
40 – 60%	0.43 ± 0.01			148 ± 5	1.047 ± 0.006	53/139		
60 – 80%	0.25 ± 0.03			139 ± 5	1.088 ± 0.005	72/137		
Pb + Pb	2760 (all)	0 – 10%	0.578 ± 0.003	99 ± 2	1.024 ± 0.004	517/285		
		10 – 20%	0.566 ± 0.003	100 ± 2	1.033 ± 0.004	467/285		
		20 – 40%	0.534 ± 0.004	101 ± 2	1.050 ± 0.004	470/285		
		40 – 60%	0.457 ± 0.005	99 ± 2	1.078 ± 0.003	373/285		
		60 – 80%	0.31 ± 0.01	96 ± 2	1.106 ± 0.002	396/283		
Pb + Pb	5020 (π, K, p)	0 – 5%	0.605 ± 0.002	93 ± 2	1.021 ± 0.005	316/90		
		5 – 10%	0.602 ± 0.003	91 ± 2	1.030 ± 0.005	303/90		
		10 – 20%	0.596 ± 0.003	93 ± 2	1.031 ± 0.005	317/90		
		20 – 30%	0.581 ± 0.003	94 ± 2	1.042 ± 0.004	268/90		
		30 – 40%	0.557 ± 0.003	93 ± 2	1.058 ± 0.004	217/90		
		40 – 50%	0.517 ± 0.004	92 ± 2	1.076 ± 0.003	189/90		
		50 – 60%	0.459 ± 0.005	92 ± 2	1.092 ± 0.003	192/90		
		60 – 70%	0.383 ± 0.009	89 ± 2	1.109 ± 0.003	177/90		
		70 – 80%	0.26 ± 0.02	88 ± 2	1.123 ± 0.003	189/90		
80 – 90%	$0_{-0}^{+0.01}$	88 ± 2	1.131 ± 0.003	174/90				

^a The measurements of π^\pm , p and \bar{p} for centrality 0-12% [29] are used as 0-10%. Λ , $\bar{\Lambda}$, Ξ^+ , Ξ^- and Ω for centrality 0-5% [43] are used as 0-10%.

^b Lack of measurements of Ω at this centrality class [43].

^c Lack of measurements of Ω [43] and intermediate p_T K^\pm [42] at this centrality class.

TABLE VIII. Extracted kinetic freeze-out parameters and $\chi^2/nDoF$ from TBW4 fit to identified particle transverse spectra in heavy ion collisions of different centralities at $\sqrt{s_{NN}} = 7.7$ GeV, 11.5 GeV, 14.5 GeV and 19.6 GeV. Results for charged pions, kaons and protons have labels ‘(π, K, p)’ behind their collision energy. All available hadrons including strange and multi-strange particles are labeled as ‘(all)’. We also fit the spectra separately for strangeness with label ‘(strange)’ and non-strange particles with label ‘(non-strange)’.

system	$\sqrt{s_{NN}}$ (GeV)	centrality	$\langle\beta\rangle$	T (GeV)	q_M	q_B	$\chi^2/nDoF$
Au + Au	7.7 (π, K, p)	0 – 5%	0.431 ± 0.008	111 ± 2	1.000 ± 0.002	1.003 ± 0.003	112/132
		5 – 10%	0.418 ± 0.009	113 ± 3	1.000 ± 0.003	1.005 ± 0.003	103/133
		10 – 20%	0.39 ± 0.01	117 ± 4	1.006 ± 0.005	1.006 ± 0.006	86/137
		20 – 30%	0.34 ± 0.02	123 ± 4	1.008 ± 0.005	1.015 ± 0.006	120/135
		30 – 40%	0.32 ± 0.02	125 ± 4	1.006 ± 0.005	1.013 ± 0.006	118/134
		40 – 50%	0.26 ± 0.03	116 ± 4	1.024 ± 0.006	1.023 ± 0.006	110/124
		50 – 60%	0.17 ± 0.08	121 ± 4	1.028 ± 0.010	1.031 ± 0.010	130/121
		60 – 70%	$0_{-0}^{+0.095}$	121 ± 4	1.033 ± 0.004	1.034 ± 0.003	95/116
		70 – 80%	$0_{-0}^{+0.095}$	116 ± 4	1.032 ± 0.005	1.025 ± 0.003	80/96
		0 – 80%	0.37 ± 0.02	105 ± 5	1.026 ± 0.009	1.020 ± 0.008	46/89
Au + Au	7.7 (all)	0 – 5%	0.426 ± 0.005	105 ± 2	1.010 ± 0.002	1.0001 ± 0.0002	234/171
		5 – 10%	0.421 ± 0.005	106 ± 2	1.009 ± 0.002	1.0001 ± 0.0002	218/172
		10 – 20%	0.399 ± 0.005	112 ± 2	1.008 ± 0.001	1.0001 ± 0.0002	186/176
		20 – 30%	0.377 ± 0.006	117 ± 3	1.004 ± 0.001	1.0001 ± 0.0003	207/174
		30 – 40%	0.362 ± 0.007	118 ± 3	1.004 ± 0.001	1.000 ± 0.001	180/173
		40 – 60%	0.32 ± 0.01	117 ± 3	1.009 ± 0.003	1.003 ± 0.002	210/157
		60 – 80%	0.24 ± 0.02	112 ± 3	1.022 ± 0.004	1.011 ± 0.004	122/128
Au + Au	11.5 (π, K, p)	0 – 5%	0.429 ± 0.006	112 ± 3	1.005 ± 0.002	1.000 ± 0.001	100/141
		5 – 10%	0.417 ± 0.006	117 ± 3	1.001 ± 0.002	1.000 ± 0.002	79/144
		10 – 20%	0.404 ± 0.006	118 ± 3	1.004 ± 0.002	1.000 ± 0.003	88/144
		20 – 30%	0.36 ± 0.02	121 ± 3	1.012 ± 0.005	1.009 ± 0.006	88/144
		30 – 40%	0.37 ± 0.01	112 ± 3	1.019 ± 0.005	1.008 ± 0.005	90/143
		40 – 50%	0.24 ± 0.03	121 ± 3	1.031 ± 0.005	1.025 ± 0.006	104/139
		50 – 60%	0.24 ± 0.03	116 ± 3	1.032 ± 0.005	1.023 ± 0.005	79/137
		60 – 70%	$0_{-0}^{+0.14}$	118 ± 3	1.044 ± 0.003	1.037 ± 0.002	86/123
		70 – 80%	$0_{-0}^{+0.08}$	116 ± 3	1.041 ± 0.003	1.034 ± 0.003	101/119
		0 – 80%	0.38 ± 0.01	109 ± 4	1.022 ± 0.006	1.017 ± 0.006	30/117
Au + Au	11.5 (all)	0 – 5%	0.433 ± 0.004	107 ± 2	1.010 ± 0.001	1.0001 ± 0.0002	169/182
		5 – 10%	0.427 ± 0.004	108 ± 2	1.011 ± 0.001	1.0001 ± 0.0003	163/185
		10 – 20%	0.418 ± 0.004	110 ± 2	1.010 ± 0.001	1.0001 ± 0.0009	152/185
		20 – 30%	0.394 ± 0.007	116 ± 2	1.010 ± 0.002	1.001 ± 0.002	133/185
		30 – 40%	0.376 ± 0.007	113 ± 2	1.015 ± 0.002	1.004 ± 0.002	124/184
		40 – 60%	0.30 ± 0.01	118 ± 3	1.022 ± 0.002	1.013 ± 0.002	154/178
		60 – 80%	0.25 ± 0.02	113 ± 3	1.028 ± 0.003	1.014 ± 0.003	131/157
Au + Au	14.5 (π, K, p)	0 – 5%	0.43 ± 0.02	116 ± 4	1.005 ± 0.007	1.002 ± 0.008	55/148
		5 – 10%	0.41 ± 0.02	117 ± 4	1.010 ± 0.007	1.008 ± 0.008	57/148
		10 – 20%	0.39 ± 0.02	116 ± 4	1.016 ± 0.006	1.015 ± 0.007	53/148
		20 – 30%	0.39 ± 0.02	114 ± 4	1.020 ± 0.006	1.015 ± 0.007	30/148
		30 – 40%	0.32 ± 0.03	122 ± 4	1.023 ± 0.006	1.022 ± 0.007	57/148
		40 – 50%	0.1 ± 0.1	116 ± 4	1.054 ± 0.009	1.055 ± 0.011	83/142
		50 – 60%	0.27 ± 0.03	111 ± 4	1.037 ± 0.006	1.028 ± 0.007	99/138
		60 – 70%	0.18 ± 0.07	118 ± 4	1.036 ± 0.008	1.03 ± 0.01	79/130
		70 – 80%	0.26 ± 0.03	111 ± 4	1.026 ± 0.006	1.012 ± 0.007	68/126
Au + Au	19.6 (π, K, p)	0 – 5%	0.44 ± 0.01	110 ± 3	1.013 ± 0.005	1.010 ± 0.006	51/145
		5 – 10%	0.42 ± 0.01	110 ± 3	1.016 ± 0.005	1.010 ± 0.006	70/141
		10 – 20%	0.40 ± 0.01	116 ± 3	1.015 ± 0.005	1.015 ± 0.006	73/141
		20 – 30%	0.36 ± 0.02	114 ± 3	1.028 ± 0.005	1.022 ± 0.005	65/141
		30 – 40%	0.30 ± 0.02	120 ± 3	1.031 ± 0.005	1.027 ± 0.006	81/142
		40 – 50%	0.15 ± 0.09	125 ± 3	1.045 ± 0.009	1.05 ± 0.01	87/140
		50 – 60%	$0_{-0}^{+0.08}$	120 ± 3	1.053 ± 0.002	1.047 ± 0.002	106/140
		60 – 70%	$0_{-0}^{+0.05}$	115 ± 3	1.055 ± 0.003	1.044 ± 0.002	135/134
		70 – 80%	$0_{-0}^{+0.05}$	113 ± 3	1.053 ± 0.003	1.039 ± 0.002	125/129
		0 – 80%	0.36 ± 0.02	108 ± 4	1.036 ± 0.006	1.032 ± 0.006	31/126
Au + Au	19.6 (all)	0 – 5%	0.453 ± 0.003	105 ± 2	1.013 ± 0.001	1.0001 ± 0.0002	162/186
		5 – 10%	0.446 ± 0.004	107 ± 2	1.013 ± 0.002	1.000 ± 0.002	158/182
		10 – 20%	0.431 ± 0.004	110 ± 2	1.015 ± 0.002	1.003 ± 0.002	165/182
		20 – 30%	0.406 ± 0.005	109 ± 2	1.022 ± 0.002	1.009 ± 0.001	146/182
		30 – 40%	0.370 ± 0.006	110 ± 2	1.027 ± 0.002	1.015 ± 0.002	198/183
		40 – 60%	0.305 ± 0.009	113 ± 2	1.035 ± 0.002	1.023 ± 0.002	230/181
		60 – 80%	0.17 ± 0.03	113 ± 2	1.048 ± 0.003	1.034 ± 0.003	197/169

TABLE IX. Same as Table VIII, but for $\sqrt{s_{NN}} = 27$ GeV, 39 GeV, 62.4 GeV and 200 GeV.

system	$\sqrt{s_{NN}}$ (GeV)	centrality	$\langle\beta\rangle$	T (MeV)	q_M	q_B	$\chi^2/nDoF$
Au + Au	27 (π, K, p)	0 – 5%	0.45 ± 0.01	114 ± 3	1.004 ± 0.006	1.004 ± 0.007	86/138
		5 – 10%	0.43 ± 0.01	111 ± 3	1.016 ± 0.006	1.013 ± 0.006	65/139
		10 – 20%	0.41 ± 0.01	114 ± 3	1.019 ± 0.005	1.017 ± 0.006	61/139
		20 – 30%	0.38 ± 0.02	112 ± 3	1.031 ± 0.005	1.026 ± 0.006	50/139
		30 – 40%	0.34 ± 0.02	112 ± 3	1.037 ± 0.005	1.028 ± 0.005	45/139
		40 – 50%	0.25 ± 0.03	114 ± 3	1.051 ± 0.005	1.043 ± 0.006	36/139
		50 – 60%	0.19 ± 0.05	114 ± 3	1.055 ± 0.006	1.044 ± 0.007	47/139
		60 – 70%	$0_{-0}^{+0.06}$	114 ± 3	1.063 ± 0.002	1.049 ± 0.002	57/139
		70 – 80%	$0_{-0}^{+0.05}$	113 ± 3	1.060 ± 0.002	1.042 ± 0.002	83/137
0 – 80%	0.39 ± 0.01	113 ± 3	1.026 ± 0.005	1.024 ± 0.006	48/136		
Au + Au	27 (all)	0 – 5%	0.464 ± 0.003	104 ± 2	1.014 ± 0.001	1.0001 ± 0.0003	211/179
		5 – 10%	0.458 ± 0.003	105 ± 2	1.014 ± 0.001	1.000 ± 0.002	158/180
		10 – 20%	0.443 ± 0.004	108 ± 2	1.017 ± 0.002	1.004 ± 0.002	139/180
		20 – 30%	0.418 ± 0.004	109 ± 2	1.024 ± 0.002	1.010 ± 0.001	127/180
		30 – 40%	0.385 ± 0.006	110 ± 2	1.030 ± 0.002	1.016 ± 0.001	101/180
		40 – 60%	0.329 ± 0.008	110 ± 2	1.040 ± 0.002	1.024 ± 0.002	100/180
		60 – 80%	0.16 ± 0.03	115 ± 2	1.055 ± 0.002	1.040 ± 0.003	124/178
Au + Au	39 (π, K, p)	0 – 5%	0.47 ± 0.01	115 ± 3	1.004 ± 0.007	1.003 ± 0.008	58/139
		5 – 10%	0.45 ± 0.01	117 ± 4	1.009 ± 0.006	1.005 ± 0.007	58/139
		10 – 20%	0.42 ± 0.01	110 ± 3	1.026 ± 0.006	1.020 ± 0.006	43/139
		20 – 30%	0.39 ± 0.01	109 ± 3	1.036 ± 0.005	1.027 ± 0.006	52/139
		30 – 40%	0.36 ± 0.02	110 ± 3	1.043 ± 0.005	1.032 ± 0.006	33/139
		40 – 50%	0.27 ± 0.03	111 ± 3	1.056 ± 0.005	1.048 ± 0.006	43/139
		50 – 60%	0.16 ± 0.06	112 ± 3	1.066 ± 0.006	1.055 ± 0.007	55/139
		60 – 70%	0.20 ± 0.04	106 ± 3	1.067 ± 0.005	1.045 ± 0.006	41/139
		70 – 80%	$0_{-0}^{+0.1}$	108 ± 3	1.074 ± 0.003	1.051 ± 0.002	59/139
0 – 80%	0.40 ± 0.01	111 ± 3	1.030 ± 0.005	1.023 ± 0.006	40/139		
Au + Au	39 (all)	0 – 5% ^a	0.470 ± 0.004	109 ± 2	1.011 ± 0.002	1.000 ± 0.001	90/180
		5 – 10% ^a	0.458 ± 0.006	111 ± 3	1.014 ± 0.003	1.002 ± 0.003	86/180
		10 – 20%	0.447 ± 0.006	107 ± 2	1.023 ± 0.002	1.008 ± 0.002	83/190
		20 – 30% ^a	0.427 ± 0.006	107 ± 2	1.029 ± 0.003	1.012 ± 0.002	88/180
		30 – 40% ^a	0.389 ± 0.007	109 ± 2	1.036 ± 0.002	1.020 ± 0.002	58/180
		40 – 60%	0.33 ± 0.01	109 ± 2	1.046 ± 0.002	1.029 ± 0.002	90/190
		60 – 80% ^a	0.21 ± 0.02	110 ± 2	1.060 ± 0.002	1.039 ± 0.003	75/180
Au + Au	62.4 (π, K, p)	0 – 10%	0.522 ± 0.005	85 ± 4	1.035 ± 0.004	1.000 ± 0.002	26/64
		10 – 20%	0.512 ± 0.009	89 ± 5	1.035 ± 0.006	1.002 ± 0.005	34/64
		20 – 40%	0.48 ± 0.01	88 ± 5	1.047 ± 0.005	1.016 ± 0.005	19/64
		40 – 80%	0.40 ± 0.02	91 ± 5	1.061 ± 0.004	1.033 ± 0.004	31/64
Au + Au	62.4 (all)	0 – 20%	0.487 ± 0.005	104 ± 3	1.024 ± 0.002	1.000 ± 0.001	113/132
		20 – 40%	0.451 ± 0.009	106 ± 4	1.034 ± 0.004	1.011 ± 0.004	84/132
		40 – 80% ^a	0.38 ± 0.01	101 ± 4	1.056 ± 0.004	1.030 ± 0.004	64/116
Au + Au	200	0 – 10% ^b	0.544 ± 0.008	79 ± 4	1.045 ± 0.004	1.006 ± 0.005	24/78
		10 – 20%	0.534 ± 0.009	80 ± 4	1.050 ± 0.004	1.012 ± 0.005	24/78
		20 – 40%	0.51 ± 0.01	78 ± 4	1.063 ± 0.004	1.025 ± 0.005	24/80
		40 – 60%	0.44 ± 0.02	83 ± 4	1.074 ± 0.003	1.043 ± 0.005	33/80
		60 – 80%	0.31 ± 0.04	88 ± 5	1.088 ± 0.003	1.062 ± 0.005	21/80
Au + Au	200 (all)	0 – 10% ^c	0.458 ± 0.006	104 ± 3	1.044 ± 0.003	1.032 ± 0.003	140/174
		10 – 20% ^d	0.458 ± 0.006	101 ± 3	1.048 ± 0.003	1.033 ± 0.003	119/172
		20 – 40%	0.425 ± 0.007	95 ± 2	1.063 ± 0.003	1.044 ± 0.003	136/176
		40 – 60%	0.30 ± 0.01	96 ± 3	1.083 ± 0.002	1.070 ± 0.003	173/176
		60 – 80% ^e	0.28 ± 0.02	92 ± 3	1.088 ± 0.003	1.068 ± 0.004	56/122

^a Lack of measurements of π^0 at this centrality class [41].^b The measurements of π^\pm , p and \bar{p} for centrality 0-12% [29] are used as 0-10%.^c The measurements of π^\pm , p and \bar{p} for centrality 0-12% [29] are used as 0-10%. Λ , $\bar{\Lambda}$, Ξ^+ , Ξ^- and Ω for centrality 0-5% [43] are used as 0-10%.^d Lack of measurements of Ω at this centrality class [43].^e Lack of measurements of Ω [43] and intermediate p_T K^\pm [42] at this centrality class.

TABLE X. Same as Table VIII, but for $\sqrt{s_{NN}} = 2.76$ TeV and 5.02 TeV.

system	$\sqrt{s_{NN}}$ (TeV)	centrality	$\langle\beta\rangle$	T (MeV)	q_M	q_B	$\chi^2/nDoF$
Pb + Pb	2.76 (π, K, p)	0 – 5%	0.590 ± 0.004	92 ± 2	1.024 ± 0.005	1.026 ± 0.006	246/212
		5 – 10%	0.588 ± 0.004	91 ± 2	1.030 ± 0.005	1.028 ± 0.006	247/212
		10 – 20%	0.584 ± 0.004	90 ± 2	1.035 ± 0.005	1.029 ± 0.006	225/212
		20 – 30%	0.574 ± 0.005	88 ± 2	1.046 ± 0.005	1.034 ± 0.006	191/212
		30 – 40%	0.557 ± 0.005	84 ± 2	1.061 ± 0.004	1.044 ± 0.005	162/212
		40 – 50%	0.525 ± 0.006	80 ± 2	1.079 ± 0.003	1.060 ± 0.004	127/212
		50 – 60%	0.485 ± 0.007	78 ± 2	1.094 ± 0.003	1.073 ± 0.004	117/212
		60 – 70%	0.441 ± 0.008	74 ± 2	1.107 ± 0.002	1.082 ± 0.003	105/212
		70 – 80%	0.40 ± 0.01	71 ± 2	1.117 ± 0.002	1.088 ± 0.003	94/212
		80 – 90%	0.33 ± 0.02	69 ± 2	1.124 ± 0.002	1.093 ± 0.003	85/212
Pb + Pb	2.76 (non – strange)	0 – 10%	0.601 ± 0.004	80 ± 3	1.037 ± 0.005	1.018 ± 0.007	197/142
		10 – 20%	0.601 ± 0.004	76 ± 3	1.045 ± 0.005	1.015 ± 0.006	170/142
		20 – 40%	0.598 ± 0.004	69 ± 3	1.060 ± 0.005	1.014 ± 0.006	106/142
		40 – 60%	0.559 ± 0.007	64 ± 3	1.090 ± 0.003	1.043 ± 0.005	57/142
		60 – 80%	0.47 ± 0.01	65 ± 3	1.113 ± 0.002	1.075 ± 0.004	60/142
Pb + Pb	2.76 (all)	0 – 10%	0.577 ± 0.003	100 ± 2	1.025 ± 0.004	1.025 ± 0.005	513/284
		10 – 20%	0.570 ± 0.004	98 ± 2	1.034 ± 0.004	1.028 ± 0.005	462/284
		20 – 40%	0.549 ± 0.004	94 ± 2	1.051 ± 0.004	1.039 ± 0.004	439/284
		40 – 60%	0.498 ± 0.005	86 ± 2	1.081 ± 0.003	1.062 ± 0.003	273/284
		60 – 80%	0.421 ± 0.008	77 ± 2	1.108 ± 0.002	1.082 ± 0.003	162/282
Pb + Pb	5.02 (π, K, p)	0 – 5%	0.596 ± 0.003	99 ± 2	1.021 ± 0.005	1.041 ± 0.006	274/89
		5 – 10%	0.596 ± 0.003	95 ± 2	1.028 ± 0.005	1.040 ± 0.005	286/89
		10 – 20%	0.591 ± 0.003	96 ± 2	1.031 ± 0.005	1.040 ± 0.005	306/89
		20 – 30%	0.580 ± 0.004	95 ± 2	1.042 ± 0.004	1.044 ± 0.005	267/89
		30 – 40%	0.565 ± 0.004	91 ± 2	1.058 ± 0.004	1.050 ± 0.004	207/89
		40 – 50%	0.535 ± 0.005	86 ± 2	1.077 ± 0.003	1.064 ± 0.004	156/89
		50 – 60%	0.492 ± 0.006	83 ± 2	1.094 ± 0.003	1.078 ± 0.003	128/89
		60 – 70%	0.447 ± 0.008	75 ± 2	1.112 ± 0.003	1.089 ± 0.003	69/89
		70 – 80%	0.38 ± 0.01	73 ± 2	1.124 ± 0.002	1.099 ± 0.003	54/89
		80 – 90%	0.32 ± 0.02	72 ± 2	1.130 ± 0.002	1.104 ± 0.003	51/89

TABLE XI. Extracted kinetic freeze-out parameters and $\chi^2/nDoF$ from BGBW fit to identified particle transverse spectra in heavy ion collisions of different centralities at $\sqrt{s_{NN}} = 7.7$ GeV, 11.5 GeV, 14.5 GeV and 19.6 GeV. Results for charged pions, kaons and protons have labels ‘(π, K, p)’ behind their collision energy. All available hadrons including strange and multi-strange particles are labeled as ‘(all)’. We also fit the spectra separately for strangeness with label ‘(strange)’ and non-strange particles with label ‘(non-strange)’.

system	$\sqrt{s_{NN}}$ (GeV)	centrality	$\langle\beta\rangle$	T (MeV)	$\chi^2/nDoF$
Au + Au	7.7 (π, K, p)	0 – 5%	0.437 ± 0.005	110 ± 2	114/134
		5 – 10%	0.428 ± 0.006	110 ± 2	107/135
		10 – 20%	0.395 ± 0.007	119 ± 2	87/139
		20 – 30%	0.378 ± 0.007	120 ± 2	132/137
		30 – 40%	0.357 ± 0.008	122 ± 2	127/136
		40 – 50%	0.328 ± 0.009	124 ± 2	127/126
		50 – 60%	0.30 ± 0.01	123 ± 2	149/123
		60 – 70%	0.26 ± 0.01	126 ± 2	107/118
		70 – 80%	0.19 ± 0.02	131 ± 2	93/98
		0 – 80%	0.401 ± 0.008	116 ± 2	53/91
Au + Au	7.7 (all)	0 – 5%	0.407 ± 0.005	118 ± 2	274/173
		5 – 10%	0.403 ± 0.005	118 ± 2	251/174
		10 – 20%	0.378 ± 0.005	124 ± 2	218/178
		20 – 30%	0.365 ± 0.005	124 ± 2	217/176
		30 – 40%	0.349 ± 0.006	125 ± 2	190/175
		40 – 60%	0.312 ± 0.006	127 ± 2	230/159
		60 – 80%	0.259 ± 0.009	127 ± 2	165/130
Au + Au	11.5 (π, K, p)	0 – 5%	0.423 ± 0.005	118 ± 2	105/143
		5 – 10%	0.416 ± 0.005	119 ± 2	80/146
		10 – 20%	0.398 ± 0.006	122 ± 2	92/146
		20 – 30%	0.375 ± 0.007	128 ± 2	95/146
		30 – 40%	0.361 ± 0.007	129 ± 2	121/145
		40 – 50%	0.302 ± 0.009	138 ± 2	153/141
		50 – 60%	0.291 ± 0.009	136 ± 2	139/139
		60 – 70%	0.25 ± 0.01	137 ± 2	130/125
		70 – 80%	0.23 ± 0.01	136 ± 2	145/121
		0 – 80%	0.403 ± 0.007	120 ± 2	40/119
Au + Au	11.5 (all)	0 – 5%	0.410 ± 0.004	122 ± 1	228/184
		5 – 10%	0.402 ± 0.004	124 ± 2	228/187
		10 – 20%	0.392 ± 0.004	126 ± 1	215/187
		20 – 30%	0.369 ± 0.005	131 ± 2	186/187
		30 – 40%	0.350 ± 0.005	133 ± 2	207/186
		40 – 60%	0.307 ± 0.006	138 ± 2	276/180
		60 – 80%	0.259 ± 0.008	137 ± 2	276/159
Au + Au	14.5 (π, K, p)	0 – 5%	0.427 ± 0.006	120 ± 2	58/150
		5 – 10%	0.416 ± 0.007	123 ± 2	61/150
		10 – 20%	0.415 ± 0.007	123 ± 2	59/150
		20 – 30%	0.403 ± 0.007	125 ± 2	44/150
		30 – 40%	0.373 ± 0.008	130 ± 2	71/150
		40 – 50%	0.344 ± 0.009	133 ± 3	139/144
		50 – 60%	0.32 ± 0.01	134 ± 3	149/140
		60 – 70%	0.31 ± 0.01	130 ± 3	108/132
		70 – 80%	0.26 ± 0.01	133 ± 3	107/128
Au + Au	19.6 (π, K, p)	0 – 5%	0.446 ± 0.005	117 ± 2	57/147
		5 – 10%	0.433 ± 0.005	120 ± 2	82/143
		10 – 20%	0.421 ± 0.006	122 ± 2	82/143
		20 – 30%	0.393 ± 0.006	129 ± 2	99/143
		30 – 40%	0.357 ± 0.007	135 ± 2	120/144
		40 – 50%	0.338 ± 0.008	136 ± 2	143/142
		50 – 60%	0.289 ± 0.008	144 ± 2	214/142
		60 – 70%	0.257 ± 0.009	145 ± 2	279/136
		70 – 80%	0.22 ± 0.01	146 ± 2	277/131
		0 – 80%	0.409 ± 0.006	124 ± 2	65/128
Au + Au	19.6 (all)	0 – 5%	0.421 ± 0.003	126 ± 1	293/188
		5 – 10%	0.414 ± 0.003	128 ± 1	283/184
		10 – 20%	0.404 ± 0.003	131 ± 1	279/184
		20 – 30%	0.382 ± 0.003	137 ± 1	322/184
		30 – 40%	0.363 ± 0.004	138 ± 1	394/185
		40 – 60%	0.330 ± 0.004	142 ± 1	550/183
		60 – 80%	0.269 ± 0.006	146 ± 2	644/171

TABLE XII. Same as Table XI, but for $\sqrt{s_{NN}} = 27$ GeV, 39 GeV, 62.4 GeV and 200 GeV.

system	$\sqrt{s_{NN}}$ (GeV)	centrality	$\langle\beta\rangle$	T (MeV)	$\chi^2/nDoF$		
Au + Au	27 (π, K, p)	0 – 5%	0.456 ± 0.005	116 ± 2	87/140		
		5 – 10%	0.448 ± 0.005	118 ± 2	73/141		
		10 – 20%	0.434 ± 0.005	122 ± 2	73/141		
		20 – 30%	0.415 ± 0.006	127 ± 2	86/141		
		30 – 40%	0.387 ± 0.007	133 ± 2	105/141		
		40 – 50%	0.354 ± 0.007	139 ± 2	145/141		
		50 – 60%	0.314 ± 0.008	146 ± 2	201/141		
		60 – 70%	0.274 ± 0.009	150 ± 2	283/141		
		70 – 80%	0.23 ± 0.01	153 ± 2	366/139		
Au + Au	27 (all)	0 – 5%	0.434 ± 0.003	125 ± 1	351/181		
		5 – 10%	0.426 ± 0.003	128 ± 1	302/182		
		10 – 20%	0.414 ± 0.003	132 ± 1	291/182		
		20 – 30%	0.394 ± 0.003	139 ± 1	329/182		
		30 – 40%	0.372 ± 0.004	143 ± 1	365/182		
		40 – 60%	0.337 ± 0.004	149 ± 1	546/182		
		60 – 80%	0.283 ± 0.005	152 ± 2	812/180		
		Au + Au	39 (π, K, p)	0 – 5%	0.468 ± 0.005	117 ± 2	58/141
				5 – 10%	0.449 ± 0.005	123 ± 2	63/141
10 – 20%	0.446 ± 0.005			124 ± 2	65/141		
20 – 30%	0.425 ± 0.006			129 ± 2	98/141		
30 – 40%	0.395 ± 0.007			137 ± 2	111/141		
40 – 50%	0.372 ± 0.007			140 ± 2	162/141		
50 – 60%	0.330 ± 0.008			147 ± 2	235/141		
60 – 70%	0.292 ± 0.009			155 ± 2	339/141		
70 – 80%	0.254 ± 0.009			159 ± 2	434/141		
Au + Au	39 (all)	0 – 5% ^a	0.454 ± 0.004	123 ± 2	132/182		
		5 – 10% ^a	0.442 ± 0.004	127 ± 2	134/182		
		10 – 20%	0.431 ± 0.004	132 ± 2	211/192		
		20 – 30% ^a	0.413 ± 0.004	137 ± 2	264/182		
		30 – 40% ^a	0.392 ± 0.004	143 ± 2	312/182		
		40 – 60%	0.355 ± 0.005	151 ± 2	632/192		
		60 – 80% ^a	0.296 ± 0.006	159 ± 2	879/182		
		Au + Au	62.4 (π, K, p)	0 – 10%	0.474 ± 0.006	125 ± 3	105/66
				10 – 20%	0.462 ± 0.007	129 ± 3	102/66
20 – 40%	0.444 ± 0.008			135 ± 3	109/66		
40 – 80%	0.39 ± 0.01			148 ± 4	193/66		
Au + Au	62.4 (all)	0 – 20%	0.445 ± 0.005	138 ± 2	216/134		
		20 – 40%	0.422 ± 0.006	145 ± 3	205/134		
		40 – 80% ^a	0.376 ± 0.008	155 ± 3	270/118		
Au + Au	200 (π, K, p)	0 – 10% ^b	0.506 ± 0.005	125 ± 2	175/80		
		10 – 20%	0.503 ± 0.006	125 ± 2	153/80		
		20 – 40%	0.483 ± 0.006	134 ± 3	281/82		
		40 – 60%	0.456 ± 0.008	141 ± 3	387/82		
		60 – 80%	0.43 ± 0.01	147 ± 4	549/82		
Au + Au	200 (all)	0 – 10% ^c	0.484 ± 0.004	134 ± 2	300/176		
		10 – 20% ^d	0.488 ± 0.004	132 ± 2	297/174		
		20 – 40%	0.467 ± 0.004	140 ± 2	519/178		
		40 – 60%	0.439 ± 0.005	144 ± 2	931/178		
		60 – 80% ^e	0.422 ± 0.007	149 ± 3	621/124		

^a Lack of measurements of π^0 at this centrality class [41].^b The measurements of π^\pm , p and \bar{p} for centrality 0-12% [29] are used as 0-10%.^c The measurements of π^\pm , p and \bar{p} for centrality 0-12% [29] are used as 0-10%. Λ , $\bar{\Lambda}$, Ξ^+ , Ξ^- and Ω for centrality 0-5% [43] are used as 0-10%.^d Lack of measurements of Ω at this centrality class [43].^e Lack of measurements of Ω [43] and intermediate p_T K^\pm [42] at this centrality class.

TABLE XIII. Same as Table XI, but for $\sqrt{s_{NN}} = 2.76$ TeV and 5.02 TeV.

system	$\sqrt{s_{NN}}$ (TeV)	centrality	$\langle\beta\rangle$	T (MeV)	$\chi^2/nDoF$
Pb + Pb	2.76 (π, K, p)	0 – 5%	0.602 ± 0.001	99 ± 1	265/214
		5 – 10%	0.600 ± 0.001	101 ± 1	274/214
		10 – 20%	0.597 ± 0.002	104 ± 1	266/214
		20 – 30%	0.590 ± 0.002	108 ± 1	272/214
		30 – 40%	0.580 ± 0.002	114 ± 1	334/214
		40 – 50%	0.566 ± 0.002	120 ± 1	472/214
		50 – 60%	0.549 ± 0.003	127 ± 2	700/214
		60 – 70%	0.526 ± 0.003	135 ± 2	1039/214
		70 – 80%	0.505 ± 0.004	142 ± 2	1371/214
Pb + Pb	2.76 (all)	80 – 90%	0.484 ± 0.005	143 ± 2	1661/214
		0 – 10%	0.589 ± 0.001	108 ± 1	541/286
		10 – 20%	0.584 ± 0.001	113 ± 1	519/286
		20 – 40%	0.569 ± 0.002	122 ± 1	601/286
		40 – 60%	0.542 ± 0.002	134 ± 1	816/286
Pb + Pb	5.02 (π, K, p)	60 – 80%	0.507 ± 0.003	146 ± 2	1496/284
		0 – 5%	0.613 ± 0.001	99 ± 1	334/91
		5 – 10%	0.613 ± 0.001	100 ± 1	338/91
		10 – 20%	0.609 ± 0.001	103 ± 1	356/91
		20 – 30%	0.602 ± 0.001	108 ± 1	336/91
		30 – 40%	0.593 ± 0.001	114 ± 1	377/91
		40 – 50%	0.579 ± 0.002	121 ± 1	519/91
		50 – 60%	0.559 ± 0.002	131 ± 1	830/91
		60 – 70%	0.545 ± 0.003	132 ± 2	903/91
70 – 80%	0.521 ± 0.004	140 ± 2	1215/91		
80 – 90%	0.502 ± 0.005	140 ± 2	1324/91		